The model of particles modes. II. Transition to a fishbone-like state triggered by global synchronization and energetic particles

A. Ghizzo, D. Del Sarto

Physics of Plasmas

The model of particles modes. II. Transition to a fishbone-like state triggered by global synchronization and energetic particles

Cite as: Phys. Plasmas **29**, 042507 (2022); https://doi.org/10.1063/5.0082394
Submitted: 15 December 2021 • Accepted: 28 March 2022 • Published Online: 26 April 2022

A. Ghizzo and D. Del Sarto

Physics of Plasmas ARTICLE scitation.org/journal/php

The model of particles modes. II. Transition to a fishbone-like state triggered by global synchronization and energetic particles

Cite as: Phys. Plasmas **29**, 042507 (2022); doi: 10.1063/5.0082394
Submitted: 15 December 2021 · Accepted: 28 March 2022 ·
Published Online: 26 April 2022

A. Ghizzo[a] and D. Del Sarto

AFFILIATIONS

IJL- UMR- CNRS 7198, Campus ARTEM, 2 allee Andre Guinier, BP 50840, 54011 Nancy Cedex, France

[a]Author to whom correspondence should be addressed: alain.ghizzo@univ-lorraine.fr

ABSTRACT

The interplay between kinetic aspects induced by energetic particles on turbulence is analyzed with a simplified model of ion-temperature-gradient-driven turbulence in magnetically confined plasmas. These topics are presented within an unified Hamiltonian framework in light of a new approach based on global phase synchronization between trapped particle modes and energetic particle modes. Numerical experiments have been carried out to elucidate concepts and physical processes of transition to a fishbone-like state triggered by energetic particles.

I. INTRODUCTION

In a previous paper,[1] we have extended a model, which describes the physics of trapped particle modes in tokamak's "banana orbits," so to include the dynamics of co-passing and counter-passing ion populations. This extended model, which accounts for the dynamics of both trapped and circulating particle modes in which gradients of temperature (and/or density) provide the source of free energy, highlights the crucial role played by synchronization in the low-frequency regime of poloidal turbulence induced by ion-temperature-gradient (ITG) instabilities or trapped electron modes (TEM). The description of trapped and circulating particle modes has been obtained after gyro-averaging particle dynamics over fast scales, which, depending on the trapped or passing character of particles, correspond, respectively, to their cyclotron and bounce (or transit) motions. This task was made easier in the framework of the Hamiltonian formalism based on the action-angle variables $J_3 - \alpha_3$ (see Refs. 2 and 3), where $J_3 = e\psi$, $\alpha_3 = \varphi - q_0\theta \equiv \alpha$. Here, ψ is the poloidal flux, and α is the angle variable that measures the particle angular motion along the magnetic field line. We have, thus, addressed the study of ITG-type instabilities in the low frequency regime from the perspective of synchronization, a nonlinear phenomenon which is ubiquitous in nature.[4,5]

From a theoretical point of view, the concept of nonlinear phase synchronization has been recently introduced in plasmas to study the formation of edge transport barriers induced by shear-flows[6] or to model the Landau damping mechanism,[7,9] or drift- wave zonal-flow turbulence in Refs. 10 and 11. Furthermore, synchronization phenomena were experimentally observed in traveling wave tubes[8] and in the edge plasma of the HL-2A tokamak,[12] where a synchronization between geodesic acoustic modes (GAMs) and magnetic fluctuations has been identified.

In Ref. 1, numerical evidence was given by synchronization of modes intervening in turbulence induced by the ITG instability. It was there shown, both numerically and theoretically that, if some conditions are met, trapped particle modes can spontaneously lock to a common frequency, which is close to the toroidal ion precession frequency. This process requires the introduction of a small population of energetic circulating ions, and it can range from "partial" to "global synchronization," i.e., it can involve just a fraction of the particle modes or all of them, depending on whether the energy of fast circulating ions is, respectively, below or above some threshold value.

Populations of fast ions can be produced in tokamak plasmas by ion cyclotron resonance heating (ICRH) and neutral beam injection (NBI), which represent two examples of heating mechanisms for fusion plasmas. It is also well known that energetic particles can strongly affect the nonlinear dynamics of the fusion plasma, even when they constitute a small fraction of the whole particle population. For example, resonances between waves and drift-orbit frequencies related to the transit or bounce motion of fast particles play an important role in transport: they can modify the structure of GAM by inducing the so-called E-GAM modes, as they have been dubbed in Ref. 29; they can stabilize the turbulence in both stellarators[30] or tokamaks;[31,32] and they can even affect the growth of tearing modes, depending on the toroidal circulating direction of fast ions.[33]

Although the theoretical model accounting for the possible transition has been discussed in Ref. 1, the numerical study therein was limited to the case of a partial synchronization. In this article, we focus instead on the transition from a partial to a global synchronization. In particular, we will show by the aid of numerical simulations that the introduction of fast passing ions generally modifies the distribution of the toroidal precession frequencies of trapped particle modes. In this way, energetic ions can change the nature of the synchronization phenomenon via a transition-like process that goes from a partial to a global synchronization. Here, we investigate the nonlinear dynamics of trapped ion modes in the presence of thermal and fast circulating ions, until the emergence of a transition associated with the global synchronization becomes manifest. The aim of this paper is to provide a conceptual overview of the transition mechanism together with synchronization aspects and by making comparison with the paradigm of the fishbone transition discussed in Ref. 13. The article has the following structure. A brief overview of the role of the synchronization model discussed in Ref. 1 and of its relevance to gyrokinetic turbulence is provided in Sec. II, where the motivations of this article are put in evidence. The concept of "particle modes," including both trapped particle modes and their circulating particle counterpart, is discussed in Sec. III. This is followed by numerical examples of the partially synchronized plasma state, which is met before the emergence of transition of the synchronization among modes in a regime referred to as the "bump-on-tail" paradigm (Sec. IV). Section V puts in evidence the differences of the partially synchronized state with the new state that emerges after the transition, as a result of the global synchronization. Associations between global synchronization aspects and the fishbone transition are discussed in Sec. VI. Conclusions are finally presented in Sec. VII.

II. RESONANCE AND KURAMOTO-TYPE SYNCHRONIZATION IN LOW FREQUENCY ION MODE TURBULENCE

If, on the one hand, a large amount of works can be found in the literature, which explore the interaction between ITG modes and TEM in the context of tokamak turbulence, it is, on the other hand, recognized since long time (see, e.g., Ref. 14) that a major role in the complex interaction between zonal flows and ITG-driven microturbulence is played also by TIMs. For example, it has been evidenced since more than two decades that coupling between ITG and TIM modes strongly affects the properties of ion thermal transport in tokamak turbulence.[15] More recently, a possible excitation of coherent structures by the interaction between ITG turbulence and TIMs has been investigated in Ref. 16 by using a reduced fluid-type model based on the use of a kinetic wave equation to describe the physics of ITG modes. Moreover, resonance between ITG-related TIMs and TEMs can lead to the generation of low frequency zonal flows that act as efficient barriers for turbulent transport.[17–20] In Ref. 19, it has also been shown that the resonance between ITG-related TIM and TEMs can be triggered by perturbations at the ion scale related to the ion polarization drift in agreement with previous results discussed in Refs. 21 and 22, where the role of polarization injection was played by a source of vorticity associated with the polarization drift averaged over a flux surface. More, in general, we can state that the resonant coupling of low-frequency modes of different nature with low wave-number TIMs, which emerge from turbulent fluctuations induced by high wave-number ITG unstable modes, strongly affects the nonlinear dynamics of tokamak turbulence.

The oscillatory behavior of the zonal flow at a very low frequency, close to the ion precession frequency, as it has been observed in Ref. 12, can be interpreted as a process of frequency synchronization between the zonal flow mode and one of the TIM modes, which can be typically chosen to have a small toroidal number, $n = 1$. This has been interpreted in Ref. 1 in light of the Kuramoto synchronization model, which we recall and discuss below in the remainder of this section. We also note that this synchronization process is reminiscent of the resonant interaction of fishbones generated by trapped ions with ions' precessional motion and leads to the emergence of a kink mode at $n = 1$. Such analogy also suggests the comparison of the phase-lock mechanism in mode synchronization with the fishbone resonance paradigm,[13] which we will discuss in Sec. VI.

A. The Kuramoto model for a system of N coupled oscillators

Research on phase synchronization phenomena traditionally focuses on ascertaining the main mechanisms responsible for the collective synchronous behavior among types of particles modes. To attain a global coherent process, interacting oscillatory elements are required. The simple model of interaction is provided by the Kuramoto model,[23,24] which can take the following form:

$$\dot{\beta}_n = \omega_n + \Gamma\lambda \sin\left(\bar{\beta} - \beta_n\right) \tag{1}$$

for $n = 1, \ldots, N$ oscillators. In this formulation, the mean-field character of the model becomes obvious. To visualize the dynamics of phases, it is more convenient to consider a swarm of points circulating around a unit circle in the complex plane in which each oscillator is represented by a point or "particle." By defining a complex order parameter $\lambda e^{i\bar{\beta}} = \frac{1}{N}\sum_{n=1}^{N} e^{i\beta_n}$, the radius $\lambda(t)$ gives a measurement of the phase coherence and $\bar{\beta}(t)$ is the average phase. Thus, when all the oscillators move in a single tight clump (see Fig. 1), λ is close to one and the system, through synchronization, acts like a giant oscillator. Conversely, if the oscillators are scattered around the circle, then λ is close to zero and no synchronous state is produced. This picture, often introduced from a pedagogical point of view in the phenomenon of synchronization between oscillators, is reminiscent of a somewhat similar scheme often used to provide a visual representation of collisionless Landau damping in plasma physics, in particular when it is interpreted in terms of phase mixing.

The Kuramoto model shows how a synchronized behavior can appear in a system, when the competitive effects of coupling (i.e., collective aspects), on the one hand, and diversity among the individual character of modes, on the other hand, are both present. This diversity in the oscillator model is taken into account by introducing a probability distribution $g(\omega)$ for describing the extension of the natural frequency of oscillators. The mean quantities $\lambda(t)$ and $\bar{\beta}(t)$ are related to $g(\omega)$ by

$$\lambda e^{i\bar{\beta}} = \int_0^{2\pi} d\beta \int_{-\infty}^{+\infty} d\omega\, g(\omega)\rho(\beta;\omega,t), \tag{2}$$

where the evolution of the density ρ of oscillators with frequency ω and phase β, at time t, is governed by the continuity equation $\frac{\partial\rho}{\partial t} + \frac{\partial}{\partial\beta}(\rho v) = 0$ in which the instantaneous velocity is defined by

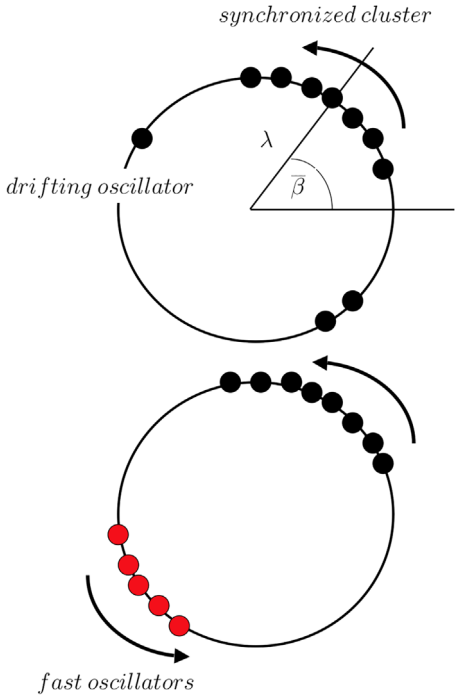

FIG. 1. Geometric interpretation of the order parameter λ in the Kuramoto model. Oscillators are represented by points moving around a unit circle in the complex plane. On top panel: the oscillator population splits into two groups: the oscillators in the bulk of the frequency distribution $g(\omega)$, lock together at the mean frequency $\bar{\omega}$, and co-rotate with the average phase $\bar{\beta}$, while those in the tail of the distribution $g(\omega)$ "drift" relative to the synchronized cluster. On bottom panel: such "drifting" oscillator population may considerably input the global synchronization of the full system through a local self-organization or (local) partial synchronization process. The introduction of fast ions may change the frequency distribution $g(\omega)$ and create a new local cluster (in red) moving at larger velocity.

$v(\beta;\omega,t)\equiv\dot{\beta}$ satisfying $\dot{\theta}=\omega+\Gamma\lambda\sin(\bar{\beta}-\beta)$, which represents the continuous limit of Eq. (1).

In the simplest setting, where the natural frequencies ω_n are drawn from a unimodal probability distribution $g(\omega)$, a classical synchronization transition, sometimes referred to as a bifurcation, is observed: at the increase in Γ, as it trespass a critical coupling strength Γ_c (usually defined in terms of $g(\omega)$ as $\Gamma_c=\frac{2}{\pi g(0)}$), a stable branch characterized by a significant number of coherent states appears, which leads to a partial synchronization. This corresponds to $\lambda<1$, the "partial synchronization" condition being characterized by the persistence of a non-negligible number of modes that are not synchronous, yet. The model described by (1), however, also admits a strongly coupled limit characterized by $\beta_n=\bar{\beta}$, which corresponds to $\lambda=1$ and which physically means that a global synchronization has occurred in which *all* oscillators are locked together in phase. More specifically, the branch of partially synchronized solutions bifurcates continuously from $\lambda=0$ at the threshold $\Gamma=\Gamma_c=\frac{2}{\pi g(0)}$. However, depending on the choice of the distribution of natural frequency $g(\omega)$, different synchronization scenarios can occur and λ acquires the asymptotic scaling,

$$\lambda\sim\sqrt{-\frac{16(\Gamma-\Gamma_c)}{\pi\Gamma_c^4 g''(0)}}\quad\text{as}\quad\Gamma\to\Gamma_c.$$

Here, g'' is the second derivative of g. Thus, the partially synchronized system bifurcates supercritically for $\Gamma>\Gamma_c$ if $g''(0)<0$ (the generic case for smooth, unimodal, and even distribution $g(\omega)$), and can bifurcate in a subcritical way for $\Gamma<\Gamma_c$ if $g''(0)>0$. Therefore, besides the usual states typical of the Kuramoto model, the so-called "incoherent" and "synchronized" states, one can find more complex dynamical occurrences, according to suitable values of the control parameter, as for instance, the emergence of many clusters, each of which contains a group of phase-locked oscillators running at a common frequency. The global synchronization is recovered as the limit case in which all these clusters are synchronized. A systematic review of the critical coupling including bimodal distributions was given in Ref. 25. As it had been already discussed in Ref. 26, one finds that the oscillator population generally splits into two groups: on the one hand, we find the oscillators in the bulk of the distribution $g(\omega)$, which lock together at the mean frequency $\bar{\omega}$ and co-rotate with the average phase $\bar{\beta}$; on the other hand, we find the oscillators in the tail of the distribution probability $g(\omega)$, which "drift" relative to the synchronized cluster. As the order parameter λ increases its value approaching unity, the number of oscillators in the tail of the distribution reduces until vanishing at $\lambda=1$.

It is generally believed that the main results concerning the global synchronization properties of a Kuramoto-type model are qualitatively independent of the precise form of the distribution $g(\omega)$, as long as it is unimodal and symmetric (usually, a Lorentzian distribution is chosen). Nevertheless, there is also evident that the "drifting" oscillator population can induce a non-trivial feedback on the evolution of the synchronization process itself and can, thus, affect the global synchronization of the whole system through a local self-organization or a partial (i.e., local) synchronization process. This occurrence is depicted in Fig. 1, bottom panel. In particular, it was reported in Refs. 27 and 28 that for certain choices of the distribution $g(\omega)$ that differ from the classic Lorentzian, unusual types of transition among different synchronization states appear.

B. The Kuramoto model for ITG-driven turbulence and the role of energetic ions in a global synchronization

The analogy between the Kuramoto model and ITG turbulence in tokamak plasmas has been presented in Ref. 1, where it has been shown [cf. Eqs. (28) and (29) therein and related discussion] that the phase β_n of the nth-Fourier component of an oscillating particle mode satisfies

$$\dot{\beta}_n=-n\omega_d(\kappa,E_i)+\frac{|\Lambda_n|}{|f_n|}\sin(\Theta_n-\beta_n).\tag{3}$$

Here, $\omega_d(\kappa,E_i)$ is the precession frequency of the ion population with adiabatic invariants κ and E_i and distribution function f, with $f_n(\psi,t)e^{in\alpha}$ being its nth Fourier component. The complex quantity $|\Lambda_n|e^{i\Theta_n}$ is the Euler representation of the n-Fourier component of the order parameter $\Lambda(\psi,\alpha,t)=-[J_{oi}^{(c)}\phi,\overline{f_s}]$ defined in terms of the Poisson bracket evaluated with respect to α and ψ, between the gyro-average operator $J_{oi}^{(c)}\phi$ for circulating ions and the distribution

function $\overline{f}_s$. We recall that, for a distribution function $\overline{f}_s = \sum_n f_{ns}(\psi, t)e^{in\alpha}$, of a species s, the Vlasov equation reads (omitting s so to simplify the notation) as

$$\frac{\partial f_n}{\partial t} + in\omega_d(\kappa, E)f_n = |\Lambda_n|e^{i\Theta_n}. \tag{4}$$

Comparison between Eqs. (1) and (3) is immediate. However, while a formal correspondence between $|\Lambda_n|$ of Eq. (3) and λ of Eq. (1) can be easily established, an important difference between the original Kuramoto model and that for TIM turbulence must be underlined: while the former (and the theory discussed in Sec. II A) refers to a finite number of oscillators (i.e., $n = 1, \ldots, N$) in the case of trapped particle modes described by Eq. (3) an infinite number of oscillators (i.e., $n = 1, \ldots, \infty$) must be, in principle, considered. Because of this and of the fact that $|f_n|^{-1}$ does not only measures the strength of the coupling but also accounts, somehow, for the number or, better, "percentage" of oscillators involved in the synchronization process (information that in the original Kuramoto's model is related to λ and $g(\omega)$, instead), it is useful to introduce a coefficient $\tilde{\Gamma} \equiv |\Lambda_n|/|f_n|$ that replaces the product $\Gamma\lambda$ and accounts for both the coupling strength (Γ in Kuramoto's model) and the level of coherence (λ in Kuramoto's model). We recall that, in the original Kuramoto's model, as the coherence of the oscillators increases, i.e., more and more oscillators become synchronized, both λ and $\Gamma\lambda$ increase. We can, thus, establish the following correspondence between terms in Eqs. (1) and (3):

$$\omega_n \quad \leftrightarrow \quad -n\omega_d(\kappa, E_i), \tag{5}$$

$$\Gamma\lambda \quad \leftrightarrow \quad \tilde{\Gamma} \equiv \frac{|\Lambda_n|}{|f_n|}, \tag{6}$$

$$\bar{\beta} \quad \leftrightarrow \quad \Theta_n. \tag{7}$$

We then see that, formally speaking, global synchronization in the turbulent plasma is allowed, in first instance, by the introduction of a population of energetic ions, provided their energies are such that a threshold value $\tilde{\Gamma}_c$ of the order parameter $\tilde{\Gamma}$ is trespassed.

A more specific picture of the mechanism with which energetic ions can make the transition possible from a partial to a global synchronization can be given by relying on the analogy with the behavior outlined in Sec. II A, about the role played by the fraction of synchronized oscillators in modifying over time the distribution of frequencies $g(\omega)$.

In the model of particle mode turbulence, the equivalent role of $g(\omega)$ is played by the repartition of the toroidal precession frequencies $\omega_{ds}(\kappa, E_s)$ in the plane of the adiabatic invariants E_s and κ. Thus, although a synchronization between different values of the frequencies $\omega_{ds}(\kappa, E_s)$ is, in principle, possible, such scenario remains, however, rare. In the absence of synchronization, the system behaves in an incoherent way where each "oscillator" (i.e., each particle mode) is running at its natural frequency. This incoherence persists until a certain level $\tilde{\Gamma}_c$ is reached, and a first step toward synchronization is obtained (a partial synchronization).

We can then expect that the introduction of fast ions could create a new local cluster of "phased-locked oscillators" (the cluster represented in red on bottom panel of Fig. 1) moving at larger velocity and, thus, change the "particle model equivalent" of the global frequency distribution $g(\omega)$. More importantly, it can be expected that the distribution $g(\omega)$ can further change in time as a consequence of the interaction of this local cluster with the bulk of the distribution of oscillators. The transition to a global synchronization can then occur when a sufficient quantity of energetic ions is injected into the plasma and the distribution $g(\omega)$ in frequencies is accordingly modified, so that the population of "oscillators" becomes coherent (condition equivalent to λ increasing its value and tending to 1), the effective coupling increases, and more and more oscillators fall into the synchronized oscillator cluster. In this way, the threshold $\tilde{\Gamma}_c$ can be crossed and the system can undergo a transition leading to a global synchronization.

The main purpose of the present article is to prove this analogy, that is, to numerically study the influence of fast ions and the effects induced by a phase synchronization process on the turbulence and the low frequency component of the zonal flow. It is in light of the considerations above that in this work, we have undertaken an investigation of the nonlinear dynamics of trapped ion modes in the presence of thermal and fast circulating ions, in order to verify the emergence of a transition from a partial to global synchronization: we will show how the introduction of fast passing ions can modify the distribution of toroidal precession frequencies $\omega_d(\kappa, E)$ and, thus, change the nature of the partial synchronization phenomenon via a transition-like process that leads to a global synchronization.

The Hamiltonian particle model that we consider in this work consists of four classes of particles: the trapped ion population, the trapped electrons, and the two circulating ion populations. These particle populations constitute four different "clusters" of "particle modes," each mode being described by a distribution function $f_{E_s,\kappa}(\psi, \alpha, t)$, which involves the adiabatic invariants E_s and κ, treated as fixed parameters. Each mode has a precession frequency $\omega_d(E_s, \kappa)$, which also depends on the energy E_s and which represents, in a way, the distribution of these particle modes in a given "cluster," according to the adiabatic invariants. The synchronization mechanism implies a process at two levels: a possible synchronization of the modes within the same cluster as well as a synchronization "extended" to all four clusters. Thus, each cluster finally has its own critical coupling threshold, represented by $\Lambda(t)$, but the effective threshold $\tilde{\Gamma} = \Lambda/f$ represents a "renormalized" threshold, thus identical to all the modes. In a partial synchronization process, all modes of the same cluster (for example, circulating ions) are not necessarily accessible. The introduction of a population of fast circulating ions makes it possible to make some of these circulating ion modes more accessible to the synchronization process, by considerably increasing the total number of synchronous modes (for all the clusters).

III. NONLINEAR EQUATIONS OF THE PARTICLE MODE MODEL

Trapped and passing particle modes have been modeled in Ref. 1 by performing a time average over fast scales corresponding to the cyclotron plus bounce motion for trapped particles or to the cyclotron plus transit motion for passing ions. Each population of particles is described by a distribution function, which we name $\overline{f}_s = \overline{f_{\kappa,E_s}}(\psi, \alpha, t)$, where E_s and κ are considered as adiabatic invariants: E_s is the energy of species s normalized to its temperature T_s, and κ is the pitch angle parameter, which depends on the nature of the particle mode. In particular, $0 \leq \kappa < 1$ for trapped particles and $\kappa > 1$ for passing ions. For a given particle species s, chosen among $\{i, e, +, -\}$, i.e., for trapped

ions, trapped electrons, co-circulating ions, and counter-circulating ions, respectively, the distribution function $\overline{f_s}$ obeys the gyrokinetic reduced Vlasov equation, where a diffusion term has been added at right-hand side for numerical applications (see later),

$$\frac{\partial \overline{f_s}}{\partial t} + \omega_{ds}(E_s,\kappa)\frac{\partial \overline{f_s}}{\partial \alpha} + \left[J_{0s}\phi, \overline{f_{is}}\right] = \partial_\psi\left(D(\psi)\partial_\psi \overline{f_s}\right). \tag{8}$$

Here, $[.,.]$ is the usual Poisson bracket defined by $[J_{0s}\phi, \overline{f_s}] = \frac{\partial (J_{0s}\phi)}{\partial \psi}\frac{\partial \overline{f_s}}{\partial \alpha} - \frac{\partial (J_{0s}\phi)}{\partial \alpha}\frac{\partial \overline{f_s}}{\partial \psi}$; $J_{0s}\phi$ is the gyro-averaged electric potential; and $\omega_{ds}(E_s,\kappa)$ is the toroidal precession frequency of particle species s. As discussed in Ref. 1, ω_{ds} depends explicitly on the type of particles, i.e., trapping or circulating. For trapped particles, for which a dependence on the charge sign $\pm$ appears, we write the precession frequency, for the species s, as

$$\omega_{ds}(\kappa,E_s) = \pm T_s \omega_{d0}\overline{\omega_{ds}}(\kappa,E_s) = \pm T_s \omega_{d0}\bar{\omega}_d^{(t)}(\kappa)E_s, \quad s=i,e, \tag{9}$$

while for co-circulating (+) or counter-circulating (−) ions, we write

$$\omega_{ds}(E_i,\kappa) = T_i\omega_{d0}\overline{\omega_{ds}}(E_i,\kappa) = T_i\omega_{d0}\left(\bar{\omega}_d^{(c)}(\kappa)E_i + \sigma_\parallel \frac{\bar{\omega}_t^{(c)}(\kappa)\sqrt{E_i}}{q_0^2\rho^*}\right), \quad s=\pm. \tag{10}$$

The labels "t" and "c" in the expressions of $\bar{\omega}_d$ refer to the type of particle, trapped, or circulating (i.e., passing), respectively. Here, $\sigma_\parallel = \pm$ and the quantities $\frac{T_i}{T_0}\omega_{d0}\bar{\omega}_d^{(c)}(\kappa)E_i$ and $\omega_{ti} = \frac{T_i}{T_0}\omega_{d0}\sigma_\parallel \frac{\bar{\omega}_t^{(c)}(\kappa)\sqrt{E_i}}{q_0^2\rho^*}$ represent, respectively, the precession frequency and the transit frequency of the population of co-passing (or counter-passing) ions. The precession frequency (at temperature T_0) is $\omega_{d0} = \frac{q_0 T_0}{e_i r_0 R_0 B_0}$, where B_0 is the minimal value of the magnetic poloidal field amplitude B_θ at $\theta = 0$, R_0 is the major radius of the tokamak. In Eqs. (9) and (10), q_0 is the safety factor, the temperature T_s is normalized to T_0, while the energy E_s is normalized to T_s. Here, $\rho^* \equiv \rho_{ci}/r_0$, with r_0 being the minor radius of the tokamak. Vlasov equations (8) are self-consistently coupled via the quasi-neutrality condition,

$$C_e(1-f_p)\left(\phi - \langle\phi\rangle_\alpha\right) + Pol.\,Terms = \sum_{s=\{e,i,\pm\}} \mathrm{sgn}(e_s)\overline{n_s}, \tag{11}$$

where

$$\sum_{s=\{e,i,+,-\}} \mathrm{sgn}(e_s)\bar{n}_s = f_p\overline{n_i}^{(t)} - f_p\overline{n_e}^{(t)} + \frac{1-f_p}{2}\sum_{\sigma_\parallel=\pm1}\overline{n_{i,\sigma_\parallel}}^{(c)} - (1-f_p). \tag{12}$$

In Eq. (12), the smoothed densities $\overline{n_s}^{(t)}$ and $\sum_{\sigma_\parallel=\pm1}\overline{n_{i,\sigma_\parallel}}^{(c)}$ are determined via the integration of the corresponding distribution functions given by Eqs. (A8) and (A9) of Appendix, respectively. The left-hand side of Eq. (12) contains different contributions of density perturbations related to trapped, co-passing, and counter-passing ions (i.e., $\{i,+,-\}$, respectively), and at right-hand side, circulating electrons are assumed to be adiabatic and polarization terms have been included in the form of

$$Pol.\,Terms = -f_p C_i \overline{\triangle_i}^{(trap)}\phi - f_p C_e \overline{\triangle_e}^{(trap)}\phi - (1-f_p)C_i\overline{\triangle_i}^{(circ)}\phi, \tag{13}$$

where $\overline{\triangle_s}^{(trap)} \simeq \frac{m_s T_s}{m_i T_i}(\rho^{*2}\partial_\alpha^2 + \delta_{bs}^2\partial_\psi^2)$ for trapped particles of species s and $\overline{\triangle_i}^{(circ)} \simeq \rho^{*2}\partial_\alpha^2 + \delta_{ci}^2\partial_\psi^2$ for circulating ions; $C_e = \frac{e}{T_e}$ and $C_i = \frac{e}{T_i}$. Here, δ_{bs} corresponds to the banana width of species s for trapped particles and δ_{ci} is the deviation of the trajectory center of ions with respect to the center of the magnetic surface.

Each distribution function $\overline{f_s} = \overline{f}_{s,E_s,\kappa}(\psi,\alpha,t)$ depends on adiabatic invariants E_s and κ, as parameters, which allows full parallelization along these directions: each distribution is normalized to one and we introduced the fraction of trapped particles $f_p = \frac{2\sqrt{2\varepsilon}}{\pi}$ to fix the total density of each class of particle mode.

IV. SCHEME AND INITIALIZATION OF NUMERICAL EXPERIMENTS

In numerical experiments, we have integrated the model equations discussed in Sec. III by using normalized quantities: the time is normalized to the inverse drift frequency ω_{d0}^{-1} and the poloidal flux ψ is given in $\triangle\psi$ units (where $\omega_{d0} = \frac{q_0 T_0}{eB_0 r_0 R_0}$ is defined at a given temperature T_0 chosen as a reference temperature). The electric potential ϕ, together with the constants C_e and C_i, are expressed in $\omega_{d0}\triangle\psi$ units.

A semi-Lagrangian scheme[34,35] has been used to integrate Eq. (8) for each class of solutions defined by the adiabatic invariants κ and E_s, as first described in Ref. 10. Details of the code are given in Ref. 1. Simulations have been initialized with equilibrium distributions [except for circulating ions where Eq. (16) is used],

$$F_{0s}(\psi) = e^{-E_s}\left[1 + \triangle\tau\bar{\omega}_d^{(s)}(\kappa)\left(E_s - \frac{3}{2}\right)\psi\right] \tag{14}$$

to which small perturbations of the type

$$\delta f_s = \phi_{pert}e^{-E_s}\sin(\pi\psi)(\cos n_1\alpha + \cos n_2\alpha) \tag{15}$$

have been added. The initial condition allows us to start an interchange instability only from an initial temperature gradient $\triangle\tau$, provided that $\triangle\tau > \triangle\tau_s$, the density being strictly equal to one since $\frac{2}{\sqrt{\pi}}\int_0^{+\infty} dE_s E_s F_{0s} = \frac{3}{2}$.

A few, further specifications can be given about the precautions taken for these numerical experiments. In simulations, the angular perturbation has been specified for the toroidal number $n_1 = 10$ and its first harmonics $n_1 = 20$. The knowledge of the marginal solution in $\sin\pi\psi$ allows us to start the ITG-type instability with a very small amplitude thanks to the numerical features of the semi-Lagrangian Vlasov solver, which uses an Eulerian grid: here, the initial "numerical noise" is given by the roundoff error of the computer, which is well below the standard noise level met in particle-in-cell (PIC) codes.

The equilibrium (14) is used for each particle species, including circulating ions. The aim is to generate a very low frequency turbulence. A population of energetic ions of density n_b and energy E_b is taken into account only for the co-circulating ion population, whose equilibrium distribution is

$$F_{0+}(\psi) = \left[(1-n_b)e^{-E_+} + n_b e^{-\left(\sqrt{E_+}-\sqrt{E_b}\right)^2}\right] \times \left[1 + \triangle\tau\bar{\omega}_d^{circ}(\kappa)\left(E_+ - \frac{3}{2}\right)\psi\right]. \quad (16)$$

A. ITG-driven turbulence and partial synchronization ($\tilde{\Gamma} < \tilde{\Gamma}_c$)

Let us first discuss some numerical simulations of ITG-driven turbulence which we have performed in order to elucidate some of the key features that are related to the inclusion of energetic ions, in conditions which lead just to a partial synchronization.

It is generally expected that the coupling of toroidal TIMs to zonal flows reduces the level of turbulence, provided the amplitude of the zonal flow mode is large enough. However, in order to model the complicated interaction of zonal flows with TIMs via a synchronization process, we have first to clarify the key points of their mutual interaction from a dynamical point of view. To this purpose, it is illuminating to first study in detail the behavior of the system as the beam energy and the beam density vary.

1. Partial synchronization induced by circulating particles in the absence of energetic ions

We first consider the limit in which no energetic circulating ions are present (we only consider thermal circulating ions), that is, we assume $n_b = 0$ in Eq. (16).

A first simulation has been performed by taking equal temperatures for ions and electrons, $T_i = T_e = T_0$, and an initial ion temperature gradient of $\triangle\tau = \frac{1}{T_i}\frac{dT_i}{d\psi} = 0.70$, for each species of particle. This is above the threshold value for the onset of the ITG instability, which is close to $\triangle\tau_s = \frac{C_e}{\xi} \simeq 0.4030$, where $\xi = 1 - \frac{3}{4}\delta_s^2 - \frac{15}{64}\delta_s^4$, $C_e = 0.40$, and $\delta_s = \delta_{be} = \delta_{bi} = \delta_{ci} \sim 0.10$. Other parameters are $\rho^* = 0.05$, a ratio aspect of $\varepsilon = 0.25$, $C_i = 0.60$, a safety factor of $q_0 = 2$, and a magnetic shear of $s_0 = \frac{r_0}{q_0}\left(\frac{dq}{dr}\right)_{r_0} = 0.8$.

We have used $N_\kappa N_E = 16 \times 120$ Vlasov equations coupled together by means of the quasi-neutrality condition. Each distribution function has been sampled with $N_\alpha N_\psi = 1025 \times 257$ grid points, and the chosen time step is $\triangle t\omega_{d0} = 0.005$.

Results of the numerical simulation are presented in Fig. 2. In order to determine what are the particle modes that drive the turbulence (and act as the "drivers"), we investigate the phasestrophy evolution for each species s, i.e., the quantity defined by $S_2 = \langle f_s^2 \rangle$. We recall that the concept of phasestrophy has been introduced in Ref. 36 and is more commonly referred to as the L^2-norm. As previously mentioned in Ref. 1, the phase-space dynamics related to the production of coherent structures during the synchronization process can be investigated and quantified in terms of the variation of the phasestrophy, allowing us to differentiate the synchronized modes from those that force the synchronization (i.e., the "pump particle modes").

The plots of $S_2(t)$ are shown in Fig. 2. We see that the first peak in the evolution of the phasestrophy S_2 takes place as related to the dynamics of the trapped ion mode, at time $t\omega_{d0} \simeq 25$ (on bottom left panel). A resonance between the population of circulating ions and TIMs occurs later in time at $t\omega_{d0} \simeq 68$ (the peak corresponding to resonance is visible for both trapped and circulating populations). These resonances are related to a nonlinear momentum transfer between the involved particle species in agreement with what has been previously discussed in Refs. 36 and 37, where the non-conservation of both entropy $S = \langle f \ln f \rangle$ and phasestrophy S_2 in Vlasov systems has been shown to be intrinsically related to phenomena such as resonant particle heating and to the emergence of coherent structures such as holes, clumps, and vortices in the phase-space. A striking contrast between electron and ion dynamics is also evident from Fig. 2: no peak is observed in the phasestrophy of electrons, which is very well conserved during the whole simulation.

Figure 2 confirms that the TIM modes appear in the system, at time $t\omega_{d0} \simeq 20$, in the nonlinear stage of the initial ITG mode but well before the emergence of a resonance peak, which is observed only later, at $t\omega_{d0} \simeq 68$, in the dynamics of both populations of circulating and counter-circulating "passing" ions. As in the case of ITG modes, it is the initial ion temperature gradient that provides the free energy for the growth of TIMs. In the nonlinear saturation phase, we can observe the emergence of coherent vortex-like structures in the distribution of the trapped ions in phase space (not shown here).

2. Partial synchronization induced by circulating particles in the presence of a sub-threshold amount of fast ions

In a second numerical experiment, we have taken into account a small population of fast ions with a beam density of $n_b = 0.10$ (normalized to the background ion density) and an energy $E_b = 5T_0$ [cf. Eq. (16)]. We can name this simulation case as the "beam-plasma" case. The other physical and numerical parameters are identical to those of the simulation presented in Sec. IV A 1. Results are shown in Figs. 3 and 4.

In spite of the inclusion of a fast ion beam, the dynamics in phase space shown in Fig. 4 is similar to that previously obtained without the beam injection, that is, the plasma dynamics is quite turbulent. The main difference with respect to the simulation case discussed in Sec. IV A 1 is in the detail of the time evolution of the phasestrophy $S_2(t)$, shown in Fig. 3. First, we exactly note that the same modes of the $n_b = 0$ case are excited but the dynamics of S_2 exhibits now more bursts in comparison with Fig. 2.

We compare the phase-space dynamics of Fig. 4 of the beam-plasma case with that of the case without the beam. The results of the two simulation cases are consistent and show that, in the beam-plasma case, the regime of interaction is dominated by the formation and growth of "clumps" with a small-size scale. This evidences the local character of the "bump-on-tail paradigm." More specifically, the introduction of a small energetic ion contribution is not a sufficient condition to trigger a transition toward a global synchronization scenario. Here, the phase synchronization process is too weak to give rise to a global outcome: each particle mode appears to be uncoupled from the others, although, of course, they are all mutually interacting through the mean electric potential $\phi(\psi, \alpha, t)$ (more specifically through the operators $J_{0s}\phi$).

Assuming the possibility of a global synchronization, these results support the existence of a threshold in the beam energy amplitude and/or in the ion beam density for a bifurcation (i.e., transition) to occur when $\tilde{\Gamma} > \Gamma_c$.

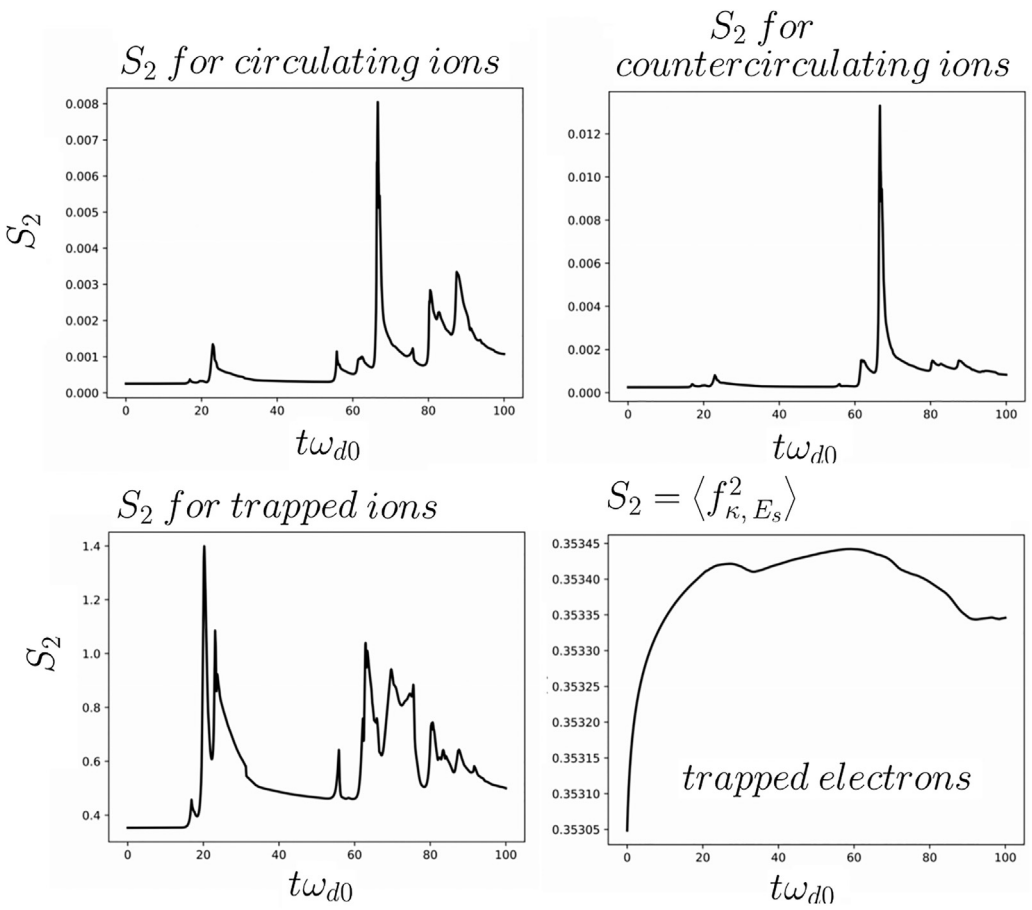

FIG. 2. Time evolution of the L^2-norm (sometimes called the "phasestrophy") $S_2 = \langle f^2 \rangle$ for trapped-ion modes (TIM) (on bottom left panel), for co-circulating ion mode (on top left panel), the counter-circulating ion mode (on top right panel), and finally for trapped electron mode (on bottom right panel). "Phasestrophy" is associated with the momentum transfer in plasma together with the formation and displacement of hole or clump structures. The dynamics of the system is first governed by the growth of TIMs associated for the emergence of the first peak at time $t\omega_{d0} \simeq 20$ on the bottom left panel. Physical parameters of the simulation are beam density $n_b = 0$, ion temperature gradient of $\triangle\tau = 0.70$, and temperatures $T_e = T_i = T_0$.

V. TRANSITION FROM PARTIAL TO GLOBAL SYNCHRONIZATION IN ITG-DRIVEN TURBULENCE

In the Kuramoto model, the critical parameter Γ_c, as well as the type of bifurcation (supercritical vs subcritical), depends on the nature of the natural frequency distribution, previously noted as $g(\omega)$ in (2). In the particle mode model, this role is played by both the frequency distribution (9) and (10) but also by the distribution function. Nevertheless, one can also consider an "effective" coupling term $\tilde{\Gamma}_c = (|\Lambda_n|/|f_n|)_c$ (i.e., equivalent in Kuramoto's model to $\Gamma_c\lambda$ the product of the coherence by the coupling term), which also contains "dynamic" features and makes it possible a feedback loop between the coupling strength and phase coherence. Thus, the introduction of a small population of circulating ions, of high energy large enough, can, in principle, modify the repartition in frequency and can lead to a global synchronization. In order to prove this concept, we have performed a further simulation in which we have increased the mean energy E_b of the beam, without changing the other physical parameters of previous simulation. We choose an energy $E_b = 10T_0$, which is twice that of the case considered in Sec. IV A 2. All other parameters of the simulations are the same of the cases discussed in Sec. IV A, except the time step that we have reduced by half for numerical stability considerations. The chosen parameters allow the nonlinear interactions among unstable modes to span a larger domain in frequencies than in the cases with $n_b = 0$. A transition from partial to global synchronization is now observed to occur on mesoscales. Numerical results of this simulation are presented in Figs. 5–10.

An overview of the trapped ion density $\langle f_i \rangle_{\kappa, E_i}$ in the $\psi - \alpha$ phase space plane is shown in Fig. 5. At time $t\omega_{d0} = 7 - 8$, at the beginning (on top panels), it is the interchange instability involving the toroidal modes $n = 2 - 3$, that dominates the dynamics of the plasma. This leads to the decrease in the amplitude of the zonal flow (not shown here) and to the growth of turbulence (see Fig. 10, bottom panel). The middle and bottom panels of Fig. 5 show that the topology of the trapped ion density changes radically at time $t\omega_{d0} = 15$ and a large-scale kink-type structure corresponding to the toroidal number $n = 1$ emerges in the phase-space (ψ, α). At later times, a seemingly

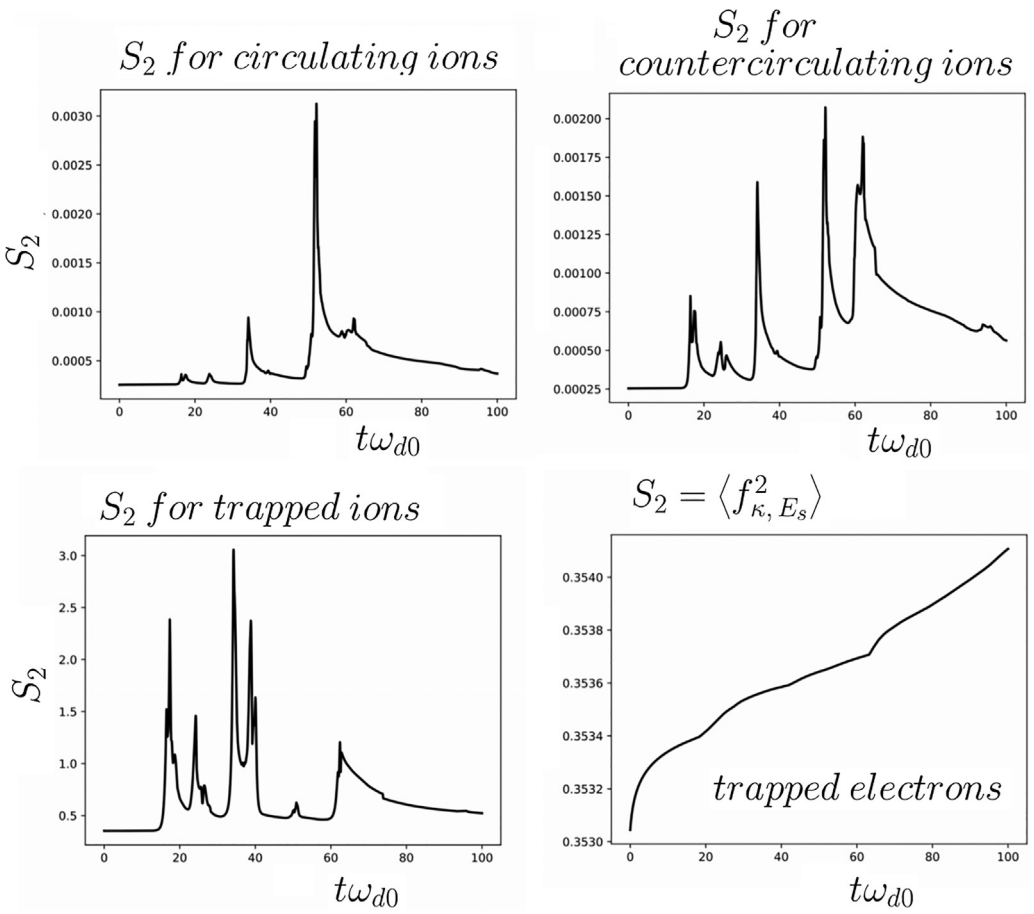

FIG. 3. Time evolution of the phasestrophy $S_2 = \langle f^2 \rangle$ for trapped-ion modes (TIM) (on bottom left panel) for co-circulating ion mode (on top left panel), the counter-circulating ion mode (on top right panel), and finally for trapped electron mode (on bottom right panel). Small differences can be observed in the dynamics of S_2, which now exhibits more bursts, in comparison to Fig. 2, without fast ion beam. Physical parameters of the simulation are beam density $n_b = 0.10 n_0$, ion beam energy of $E_b = 5T_0$, ion temperature gradient of $\triangle\tau = 0.70$, and temperatures $T_e = T_i = T_0$.

metastable state is reached, which is characterized by a coherent phase-space cavity-like structure that drifts at constant velocity over a long time interval. At the same time, finer and finer filaments develop inside the cavity-like structure (as it can be seen at time $t\omega_{d0} = 15 - 30$), and the distribution of ions inside of it is smeared out by phase-mixing and coarse-graining in a scenario similar to that encountered in Landau damping. The coherent structure displayed in the phase-space in Fig. 5 corresponds to a globally synchronized state, locked to the phase of the $n = 1$ ion mode. This result is coherent with the theoretical expectations, and we can, thus, infer that the chosen numerical parameters correspond to a value $\tilde{\Gamma} \gtrsim \tilde{\Gamma}_c$.

It is illuminating to compare in detail the behavior of populations of trapped ions and co-passing ions in the $\psi - \alpha$ plane, at two different values in energy, shown in Fig. 6. First, the energetic particle mode frequency continuously readjusts to the resonance condition $\omega \sim n\omega_d(E_s, \kappa)$. The nonlinear evolution of the system is now dominated by a resonant fast ion mode whose phase is locked with the TIM wave. This maximizes the wave-fast ion interactions and the corresponding energy transfer. In Fig. 6, we have plotted, at time $t\omega_{d0} = 40$, the distribution of co-passing ions, for an energy $E_i \sim 6$ on top panel. The middle panel represents the dynamics of the corresponding "pump" particle mode (TIM) at the same energy E_i. We clearly see that a resonant process takes place in the trapped ion distribution, a process driven by fast ions. The plots on top panel show strong distorsions of both the thermal trapped ion distribution (middle panel) and of the energetic distribution function (co-circulating distribution). This resembles to the dynamics of trapped ions taken at a higher value in energy, $E_i \sim 9$, plotted on the bottom panel. The transport of co-passing ions seems to occur in avalanches, i.e., as a secular process, accompanied by a (energetic) particle mode, convectively amplified, from an energy $E_i \sim 9$, toward $E_i \sim 6$, i.e., to regions of the parameter space that correspond to smaller energies but have higher densities. Thus, an avalanche-type process consists of a wave packet that is convectively amplified as it moves radially in ψ (toward regions of higher densities) by locking the phase with a TIM that acts as a pump energy source.

Figure 7 illustrates the temporal behavior of the phasestrophy for different classes of particle modes: as the transition occurs, there is no

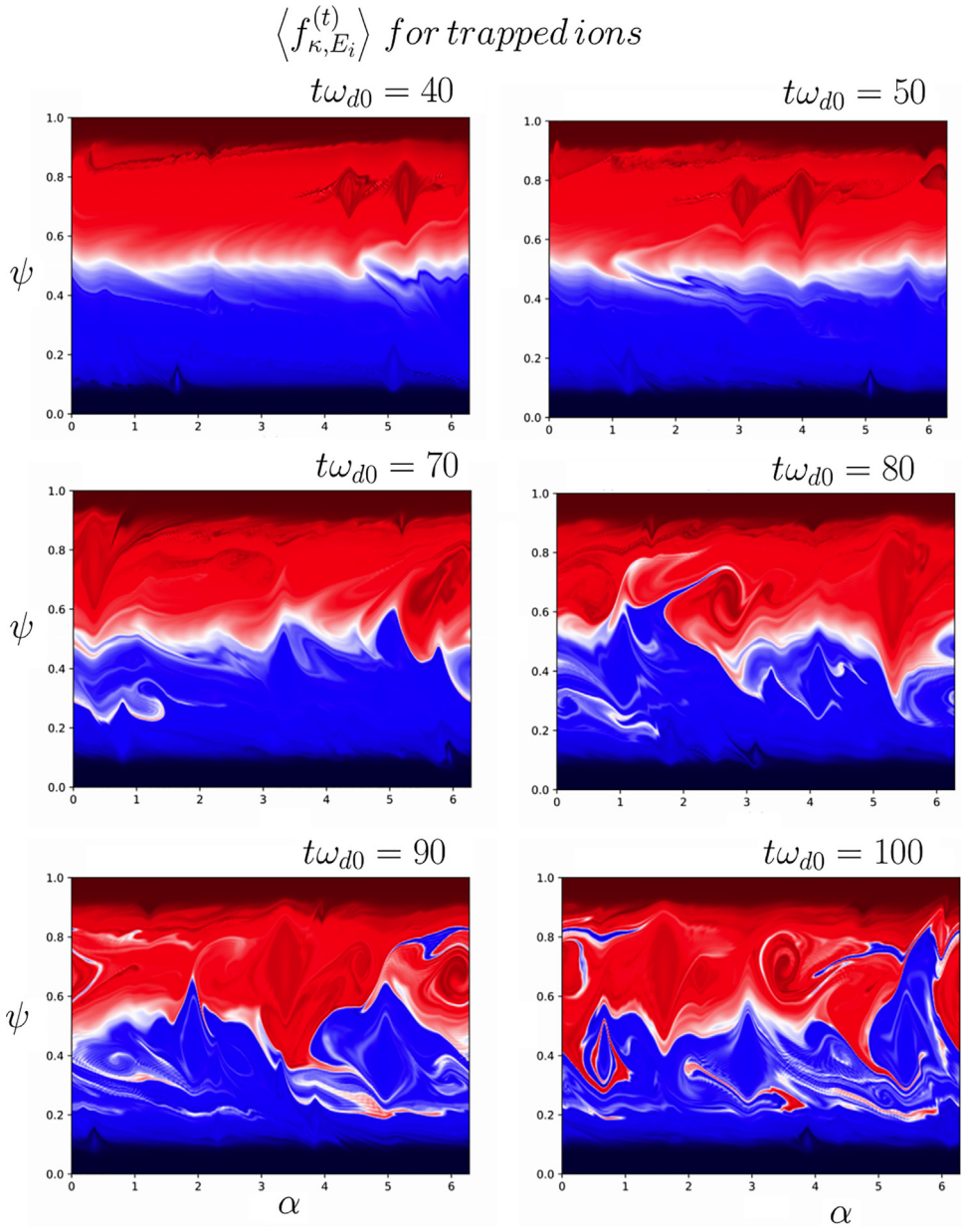

FIG. 4. Phase space representation of the distribution function of trapped ions. We clearly observe the emergence of a strongly turbulent state where coherent structures similar to the clump-hole appear in the phase space, which suggests that a regime dominated by the bump-on-tail paradigm introduced by Berk and Breizman and Cheng and Zonka. Physical parameters of the simulation are beam density $n_b = 0.10n_0$, ion beam energy of $E_b = 5T_0$, ion temperature gradient of $\triangle\tau = 0.70$, and temperatures $T_e = T_i = T_0$.

local formation of clumps and the phasestrophy exhibits a slow variation without the generation of peak: S_2 evolves in a similar way for different classes of particles except for the co-circulating ion populations (on top left panel), which includes the fast ion contribution.

An example of the energy variation that we can attribute to the transition occurring for $\tilde{\Gamma} \sim \tilde{\Gamma}_c$, is shown in Fig. 8. Here, we have plotted the time evolution of the kinetic energy $E_{kin,i}$ of trapped ion on the top left panel, of the kinetic energy $E_{kin,+}$ of the co-passing ions on the top right panel, of the turbulence energy E_{turb}, on the bottom left panel, and finally of the zonal flow E_{ZF} on the bottom right panel. These quantities have been computed by using expressions (A1), for the kinetic energy [combined with (A4) or (A5) depending on the nature of particle mode], and (A2) and (A3) for the turbulent and zonal flow energy, respectively.

The trapped ion mode plays the role of the particle pumping mode (although the counter-circulating ion mode displays a similar behavior, but at a weaker level), transferring energy to the turbulence component E_{turb}. The latter reaches a quite large amplitude, which is two thousand times larger in comparison to the amplitude measured in the absence of the fast ion beam. This occurs together with a strong decrease in the E_{ZF} component, which follows the behavior of the kinetic energy of trapped ions.

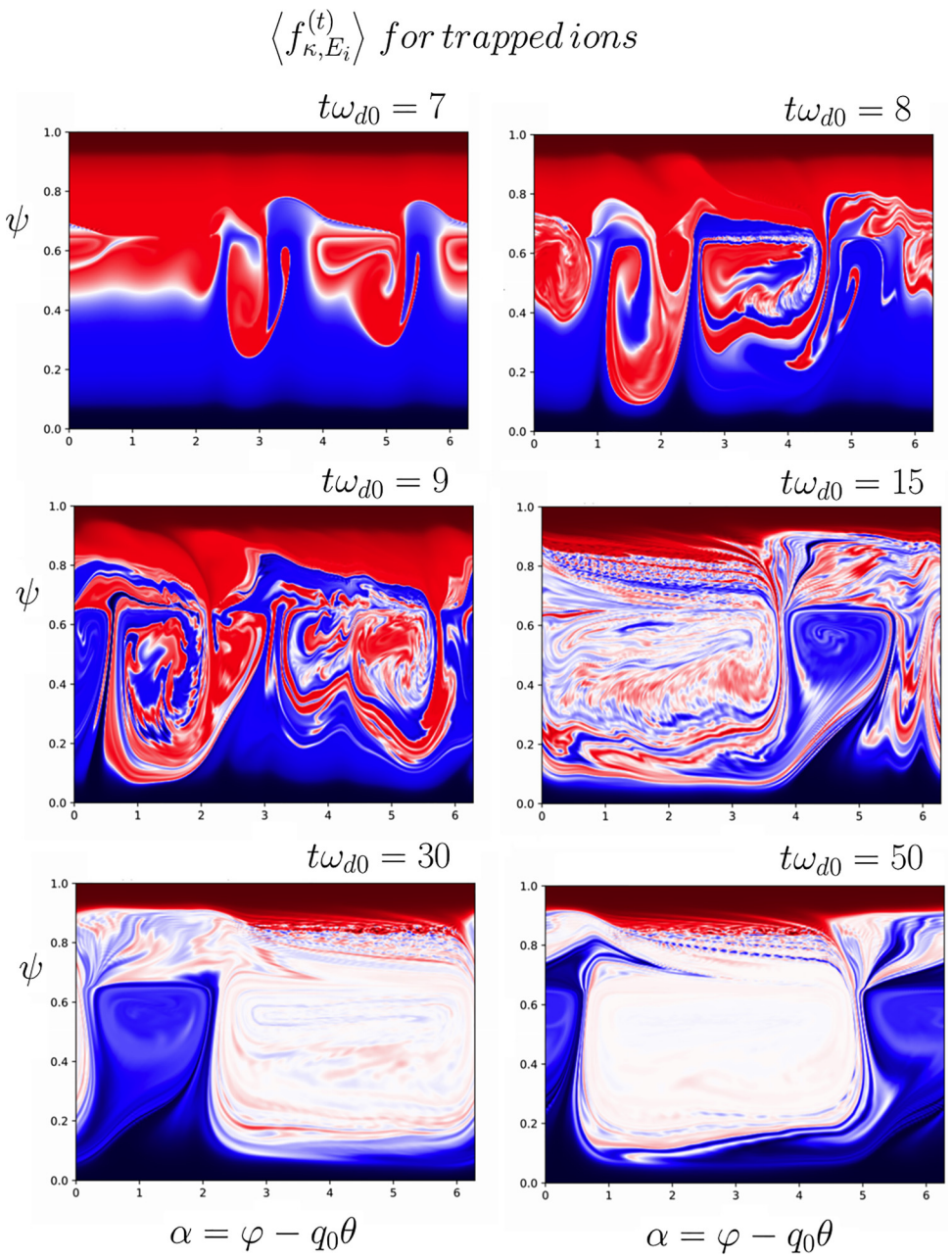

FIG. 5. $\psi - \alpha$ phase space representation of the trapped ion density $\langle f_i \rangle_{\kappa,E}$. At time $t\omega_{d0} = 7 - 8$, at the beginning (on top panels), it is the interchange instability that dominates the dynamics of the plasma. When the transition takes place the topology is strongly modified leading to the formation of a cavity. Physical parameters of the simulation are beam density $n_b = 0.10n_0$, ion beam energy of $E_b = 10T_0$, ion temperature gradient of $\triangle\tau = 0.70$, and temperatures $T_e = T_i = T_0$. The time step has been reduced by half compared to the simulation in Figs. 3 and 4.

The numerical results presented so far can be interpreted in terms of the transition from partial to global synchronization, as it is outlined in Sec. II B. Before the transition, the system is constituted of two populations: the plasma bulk and a beam of high velocity particles. In the Hamiltonian representation used here, these populations can be likened to two clusters of oscillators (Fig. 1, bottom panel), one moving at low velocity and a second cluster (shown in red in Fig. 1), moving at higher velocity. The main cluster, formed by trapped particles, is pushed or accelerated by the second one, which, in turn, undergoes a deceleration, induced by the first cluster, until both get the same angular velocity. A global synchronization is then achieved. In the Hamiltonian ITG-driven turbulence model, the velocity of each cluster

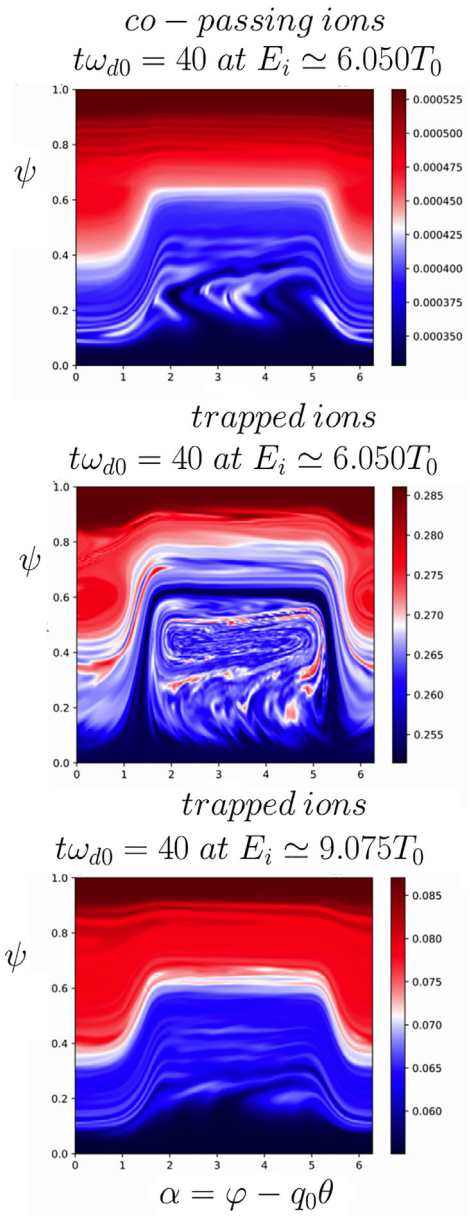

FIG. 6. Illustration of the behavior in the $\psi - \alpha$ phase space of trapped ions (on middle and bottom panels) and co-passing ions (on top panel) at two values in energy at time $t\omega_{d0} = 40$. The dynamics convectively amplified (energetic) particle mode from an energy $E_i \sim 9$, toward $E_i \sim 6$, i.e., to regions of smaller energies but with higher densities. Physical parameters of the simulation are beam density $n_b = 0.10n_0$, ion beam energy of $E_b = 10T_0$, ion temperature gradient of $\triangle\tau = 0.70$, and temperatures $T_e = T_i = T_0$. The time step has been reduced by half compared to the simulation in Figs. 3 and 4.

is determined by its frequency $\omega_d(\kappa, E_i) = \omega_{d0}\bar{\omega}_d(\kappa)E_i$. The cluster constituted by the energetic particles, thus, has a velocity, which is the higher, the larger is the cluster energy. Based on this argument, one can, thus, expect a global synchronization to occur for a toroidal number $n = 1$, when $\omega_d(\kappa, E_i) = \omega_{d0}\bar{\omega}_d(\kappa)E_i \sim \frac{3}{2}T_0\omega_{d0}\langle\bar{\omega}_d(\kappa)\rangle_\kappa \sim 2.5\omega_{d0}$, using a mean value of $\langle\bar{\omega}_d(\kappa)\rangle_\kappa \simeq 1.66$ for the TIM (cf. Fig. 10 below).

In order to evaluate the Fourier components of the corresponding order parameter $|\Lambda_n|$ [cf. Eq. (4)] and to estimate the synchronized frequency, in Figs. 9 and 10, we have represented the time evolution of the dominant term in the Poisson bracket $[-J_0\phi, f]$, that is, the quantity $\langle -\frac{\partial J_{0i}\phi}{\partial\alpha}\frac{\partial\bar{f}_i}{\partial\psi}\rangle$, averaged over κ, E_i and over the phase space variables ψ and α.

In Fig. 9, we have represented, at the top, the evolution of the quantity $\Lambda(t) \simeq \langle -\frac{\partial J_{0i}\phi}{\partial\alpha}\frac{\partial\bar{f}_i}{\partial\psi}\rangle$ as a function of time for two different values of the shifted energy of the beam $E_b = 5T_0$ (at left) and $E_b = 10T_0$ (at right). The lower figures show the frequency spectrum of this quantity for the two simulations considered. We can see that the Λ coupling coefficient presents a complex dynamics with the emergence of turbulence bursts during the time evolution, which correspond mainly to the peaks observed in the dynamics of the phase-trophy in Fig. 3 (for the left column). In the first simulation, this coefficient remains bounded and does not exceed a maximum threshold of $\Lambda_{max} \simeq 0.001$. When the average energy E_b of the beam is increased, the coupling coefficient attains the larger value $\Lambda_{max} \sim 0.008$. Based on the previous discussion, we can say that this value exceeds the critical threshold that leads to the bifurcation toward total synchronization. The corresponding frequency spectra (bottom figures) show a synchronization mechanism where only one frequency (related to the toroidal mode $n = 1$) has emerged resulting from the global synchronization (on bottom right panel). In contrast, higher frequencies were observed to persist in the $E_b = 5T_0$ simulation case.

We can also observe an identical spectrum for all four clusters of particle modes in Fig. 10. The spectrum $\Lambda(\omega)$ exhibits a dominant peak at the mean, trapped ion frequency $\omega_d^{trapped} \sim \frac{3}{2}T_0\omega_{d0}\langle\bar{\omega}_d(\kappa)\rangle_\kappa \sim 2.5\omega_{d0}$ in perfect agreement with previous estimates. The same plot is also visible the contribution of the zonal flow at $\omega_{ZF} \sim 0$, which is driven by the Reynolds stress $\frac{1}{2}\langle\frac{\partial\phi}{\partial\alpha}\frac{\partial\phi}{\partial\psi}\rangle_\alpha$. We observe the appearance of a high frequency close to $\omega \simeq 10\omega_{d0}$ associated with the initial co-passing fast ions $\sim\frac{E_b}{T_0}\omega_{d0}\langle\bar{\omega}_d(\kappa)\rangle_\kappa \sim 12$–$15\omega_{d0}$. Notice also the emergence of the mode $n = 2$ in the spectrum $\Lambda(\omega)$ of the trapped electron population.

Thus, these phase-locked fast ions that play a crucial role in avalanche process, as previously remarked by Chen and Zonca in Ref. 13, are also responsible of global synchronization aspects observed in simulations. The synchronization process leads to a spread in the frequency of the pump mode, which is partly due to the trapped particles (according to an acceleration mechanism of the thermal oscillator cluster in Fig. 1) and partly to an inverse cascade in energy associated with an avalanche process (in turn, due to a slowdown of the fast oscillator cluster).

VI. DISCUSSION: SYNCHRONIZATION, ENERGETIC IONS, AND FISHBONE PARADIGM

We have shown how resonance between energetic particles and a few, small-wave number particle modes (TIMs), which are present in a turbulent-like spectrum, can lead to the global synchronization of the ensemble of modes and to the emergence of time-oscillating zonal flows. As preliminarily discussed in Ref. 1, where it has been shown how Kelvin–Helmholtz-type fluid modes can take part to the process,

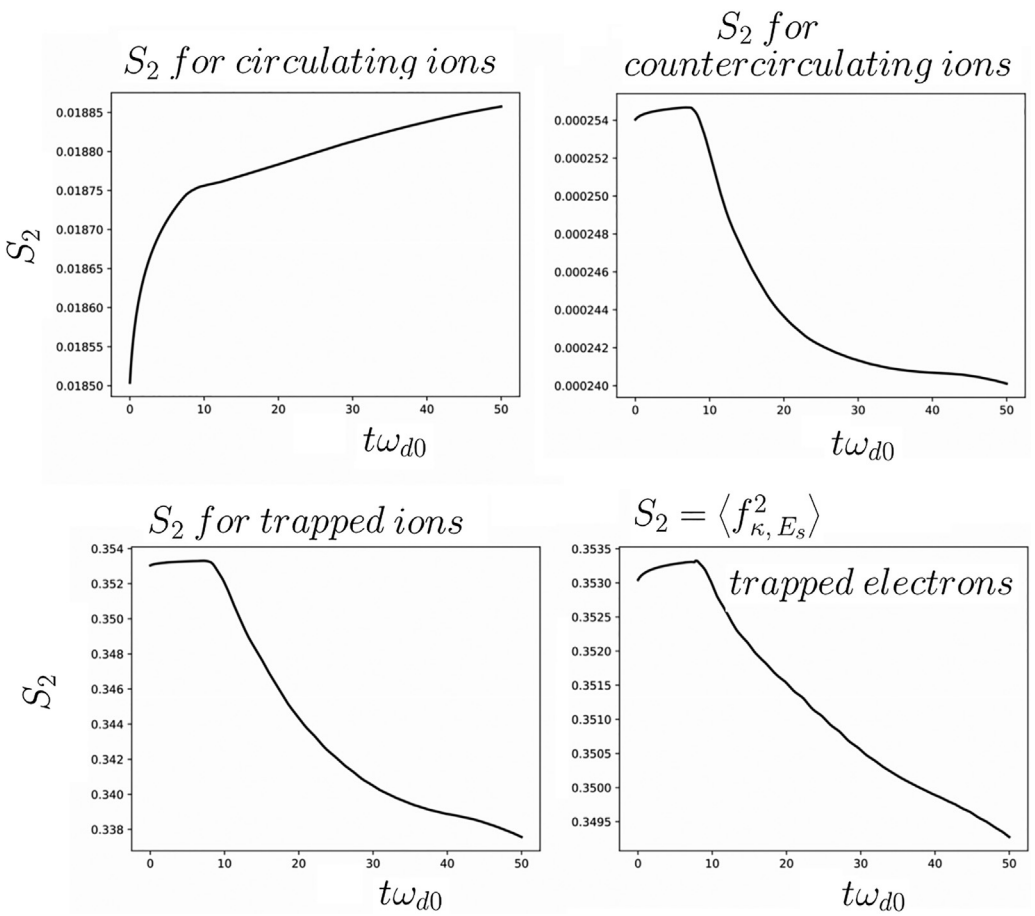

FIG. 7. Illustration of the temporal behavior of the phasestrophy when the transition takes place. S_2 evolves in a similar way for different classes of particles except for co-circulating ion populations (on the top left panel), which contains the fast ion contribution. Physical parameters of the simulation are beam density $n_b = 0.10n_0$, ion beam energy of $E_b = 10T_0$, ion temperature gradient of $\triangle\tau = 0.70$, and temperatures $T_e = T_i = T_0$. The time step has been reduced by half compared to the simulation in Figs. 3 and 4.

too (although, for this case, we have given numerical proof only of a partial synchronization), the basic mechanism behind this phenomenon appears to be quite general and shows resemblances with further models of interaction between energetic particles and other low-wavenumber modes, like, e.g., the fishbone paradigm.[41] In this section, we clarify this point after having recalled the key features of other known models of interaction between wave and fast particles in collisionless plasmas.

It is now well known that energetic particles can affect the high frequency regime of zonal flows, that is, the geodesic acoustic modes (or GAMs[38,39]). The theoretical approach developed by Fu in Ref. 29, based on both MHD and kinetic aspects induced by energetic particles, has shown that such an interaction leads to the emergence of a new mode, the so-called "energetic-particle induced GAM" (EGAM) with a frequency, which is about half that of a usual GAM. Another important theoretical prediction has been made in this context by Chen, in Ref. 40, who -evidenced the existence of the so-called "energetic-particle continuum modes" (EPM). These modes can emerge in a variety of different forms, the best known, and first observed of which, is the fishbone mode.[41] This is an internal kink mode with toroidal number $n = 1$, which can be excited by the resonance of ions' toroidal precession with fast trapped particles. In fact, both fishbones and energetic particle continuum modes can maintain a high level of interaction through resonance between waves and fast particles: the phase locking with resonant particles is maintained via frequency chirping. Such a kind of phase locking was introduced by White *et al.* in the fishbone model so to explain the secular transport mechanism.[42]

As remarked by Chen and Zonca in their review article,[13] the nonlinear interactions driven by energetic particles in tokamak plasmas can be classified according to two main "paradigms": the "bump-on-tail approach," usually met in the one-dimensional Vlasov–Poisson modeling[43,44] and the "fishbone" or "energetic particle continuum mode approach."

The bump-on-tail approach is characterized by the formation of holes and clumps in the phase space. By considering transport on a local scale, the "clump" concept has been introduced by Dupree in Refs. 46 and 47, while the notion of phase space hole is related to a generalized Bernstein–Greene–Kurskal (BGK) equilibrium.[48]

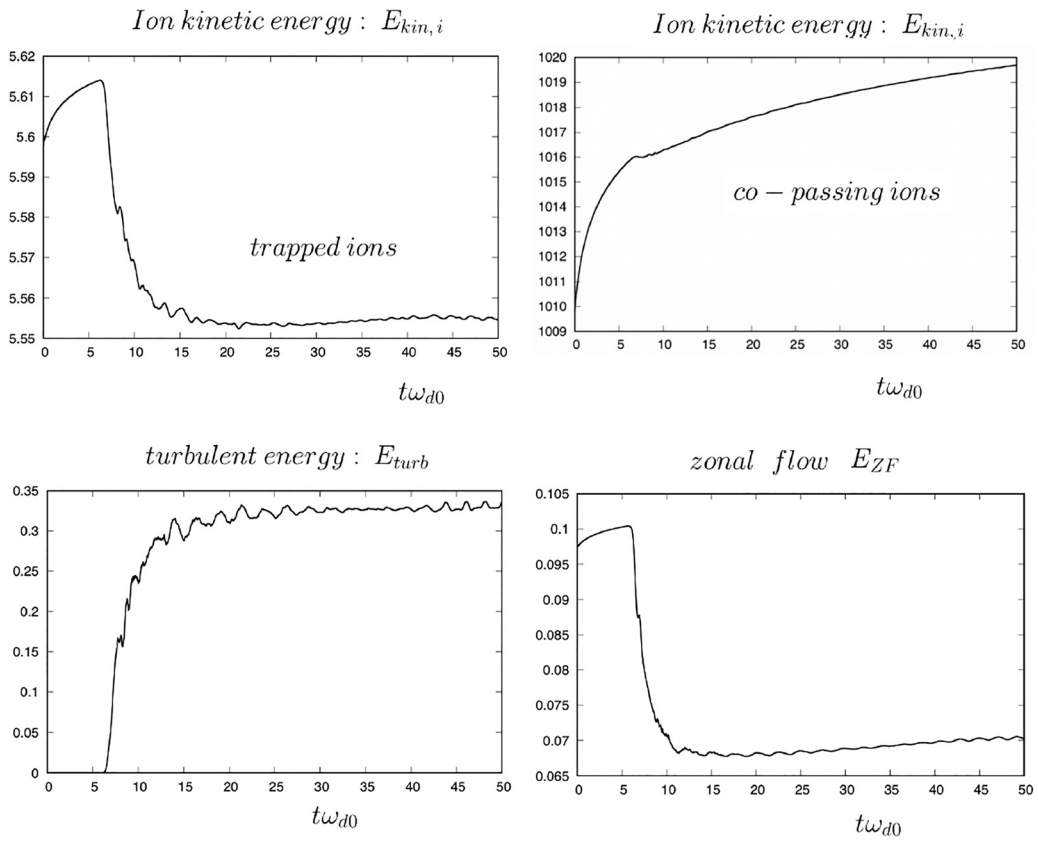

FIG. 8. Illustration of the energy variation at the transition $\tilde{\Gamma} \sim \tilde{\Gamma}_c$: the kinetic energy of trapped ions $E_{kin,i}$ (on top left), of the co-passing ion population $E_{kin,+}$ (on top right), of the turbulent energy E_{turb} (on bottom left), and of the zonal flow E_{ZF} energy (on bottom right) are plot vs time. The trapped ion mode plays the role of the particle pumping mode, transferring energy to the turbulence E_{turb} component and to the co-passing ion population. Physical parameters of the simulation are beam density $n_b = 0.10n_0$, ion beam energy of $E_b = 10T_0$, ion temperature gradient of $\triangle\tau = 0.70$, and temperatures $T_e = T_i = T_0$.

Berk *et al.* used in Ref. 45 a simplified approach to study these phenomena: they have explored the classic bump-on-tail problem of a distribution function that excites an electrostatic wave. The insight brought by their approach is the fact that the presence of a spatial gradient of the canonical toroidal momentum $P_\varphi = e\psi$, which drives the energetic particles instabilities, is analogous to the velocity-gradient that finally drives the formation of the BGK holes in the standard beam-plasma[53] or two-stream instability.[49,50]

On the other hand, the approach based on energetic particle continuum modes grounds on their global and resonant character. The energetic particle modes, by tapping energy from the regions with steeper spatial gradients via phase-locking with fast particles, can undergo a modification of their own structure, which further enhances the interaction between waves and the fast particles themselves. As predicted by White *et al.*,[42] energetic particle modes can, thus, adapt their own frequency and modify the beam-plasma instability so that the motion of particles becomes secular, as long as a wave-particle phase-locking is maintained: this process is often referred to as the "mode-particle pumping" and it has been used to explain the particle losses due to fishbones.[42]

This process seems quite general and is also encountered in the interaction of a high intensity laser wave with a plasma, in particular in the case of stimulated Raman scattering (SRS). In this scenario, the electromagnetic wave plays the role of a pump wave that transfers its energy to a plasma wave. SRS generally involves the parametric interaction between the three modes involved: the electromagnetic pump, the scattered mode (so-called Stokes wave), and a plasma (Langmuir or Bohm–Gross) wave. A tuning both in the frequency and in the wave number is then necessary. In the so-called kinetic regime of SRS, the matching conditions between the wave numbers and the frequencies of various modes can be maintained as the former vary (see Ref. 51), and this can be shown to occur also in the case of laser propagation in a parabolic plasma:[52] one can observe drifts in both the frequencies and the wave vectors, which maintain the matching conditions and lead to a self-resonance mechanism by phase locking.

The global phase-synchronization, which we have evidenced in Sec. V, can be then equivalently interpreted as a transition from a local transport in the "beam-plasma" scenario to the mesoscale transport in the "fishbone" paradigm. In this light and in spite of the fact that the model we have developed for ITG turbulence is intrinsically electrostatic, whereas fishbone modes correspond to magnetic perturbations, when the transition to global synchronization takes place it is possible to consider the (TIM) particle mode modified by fast ions as an electrostatic analogous of a fishbone mode. Conversely, this suggests that

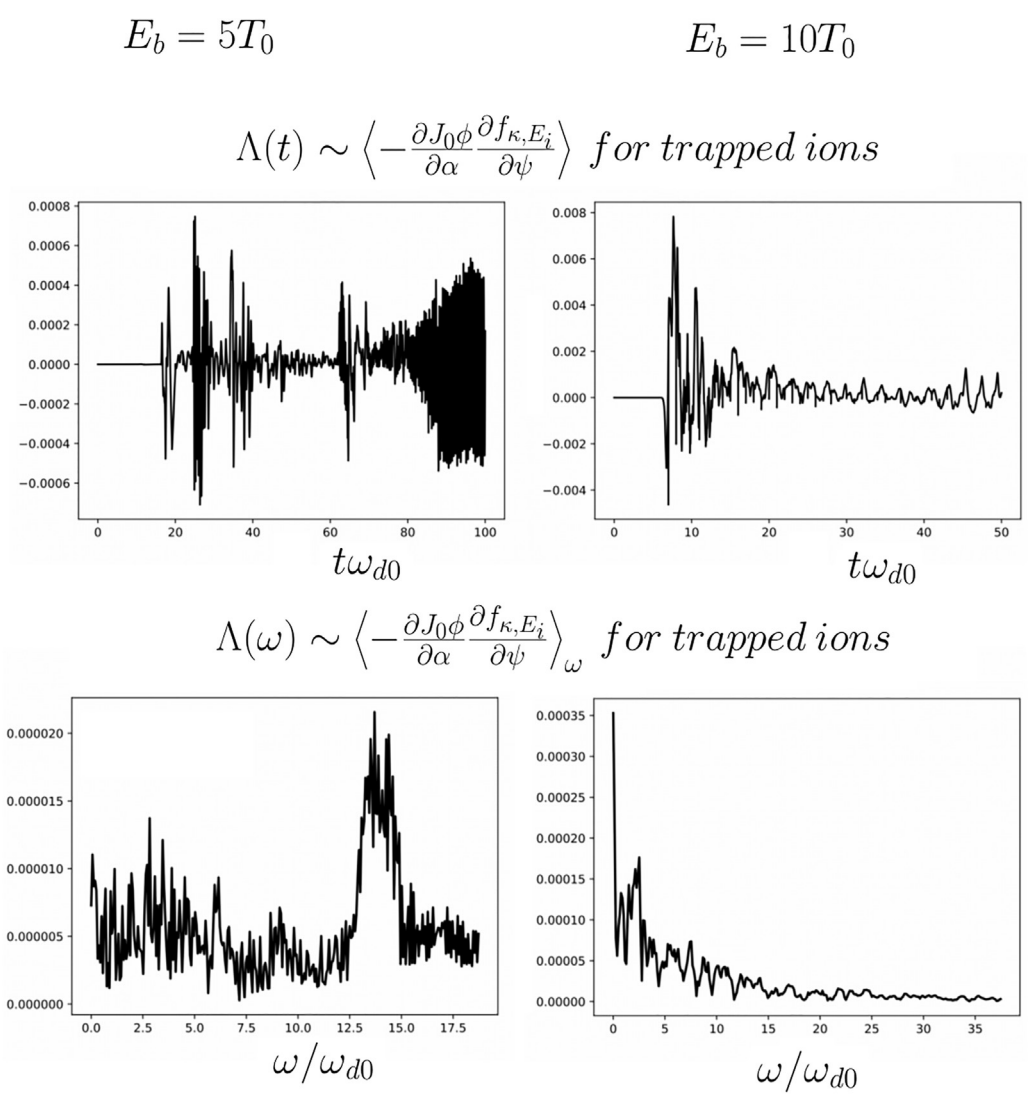

FIG. 9. Plot of $\Lambda(t) \simeq \langle -\frac{\partial J_0 \phi}{\partial \alpha} \frac{\partial \bar{f}_i}{\partial \psi} \rangle$ vs time, calculated for the population of trapped ions, for two different values of the beam energy: before the transition for $E_b = 5T_0$ (left column) and $E_b = 10T_0$ (right column) when the system has achieved global synchronization. The lower frames show the frequency spectrum of $\Lambda(t)$ for the two simulations considered. On the top left panel, the Λ coupling coefficient presents a complex dynamics with turbulence bursts during the time evolution, which corresponds mainly to the peaks observed in the dynamics of the phasestrophy in Fig. 3 (bottom left panel). Before the transition, the spectrum in the frequency is broad with a high-frequency contribution (TIM modes). On top right panel, Λ may exceed the critical threshold leading to the bifurcation toward total synchronization. Its spectrum in the frequency (on bottom right) exhibits a synchronized aspect with only a shifted value toward low frequencies.

the fishbone resonance scenario could be interpreted in light of a Kuramoto-type global synchronization. In this regard, an interesting aspect of the transition from partial to global synchronization, which we have evidenced in the simulations of ITG turbulence of Sec. V, is its dependence on a single physical parameter: the beam energy shift, E_b, with respect to the energy of the bulk of other circulating ions, E_+ (we recall that the density of the fast beam, n_b, has been kept fixed in all simulations that we have discussed). Since the progressive increase in this energy shift leads to a bifurcation scenario, once a threshold value is trespassed (i.e., the value that makes $\tilde{\Gamma} > \tilde{\Gamma}_c$), it would be interesting to investigate if an analogous "simple" mechanism could be behind the transition from a bump-on-tail to a fishbone scenario for electromagnetic-type modes, which is what the results we have here discussed for electrostatic ITG turbulence seem to suggest.

VII. CONCLUSION

We have described the dynamics of transition of ITG-driven turbulence from a regime where transport is dominated by incoherence among modes (i.e., "a strongly turbulent" regime) to a regime where meso-scale coherent structures appear (i.e., low frequency zonal flows), which oppose to turbulent transport. The two regimes can be interpreted in light of a Kuramoto-type synchronization model, which had

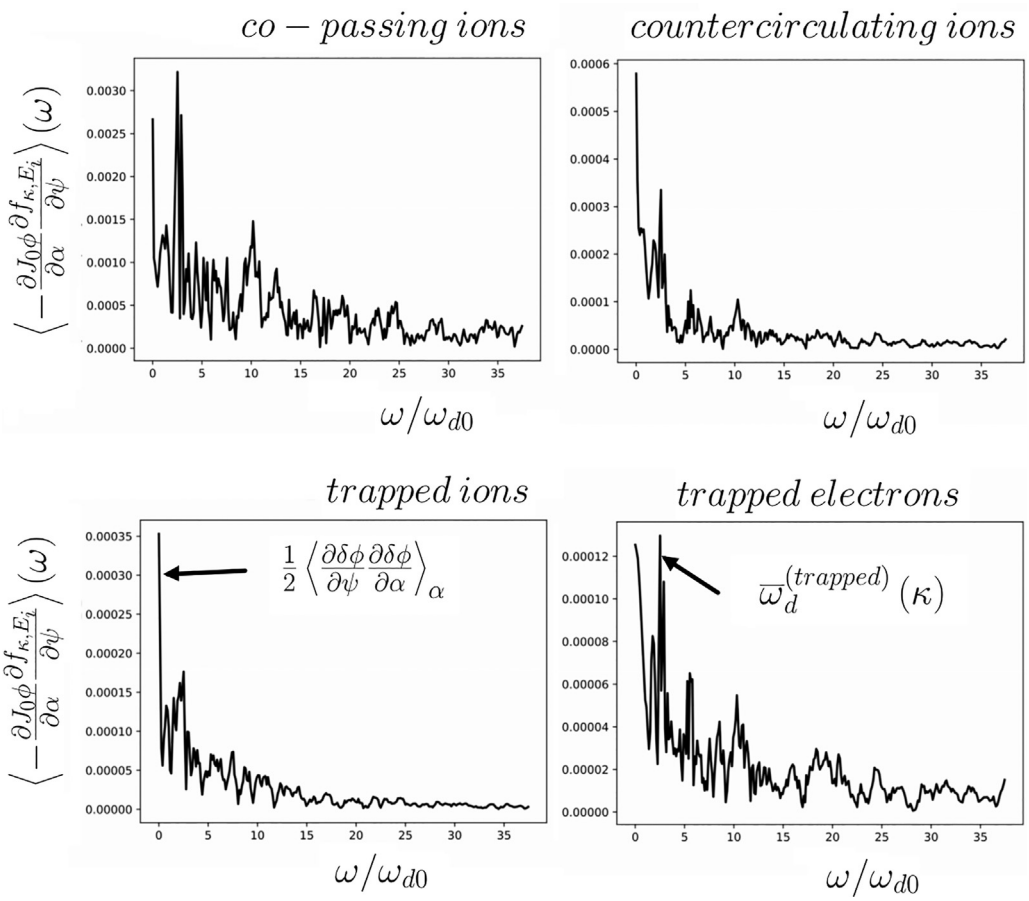

FIG. 10. Illustration of the spectrum of the quantity $\langle -\frac{\partial J_0\phi}{\partial\alpha}\frac{\partial\bar{f}_i}{\partial\psi}\rangle$, the average operator $\langle . \rangle$ being made on all variables κ, E_s, ψ, and α. This function gives an estimation of the order parameter $\langle R_s(\psi,\alpha,t)\rangle_{\psi,\alpha}$ in the synchronization mechanism induced by the "pump" driver term (the trapped ion mode, shown on the bottom panel at left). On top, at left, the co-passing ion mode contains the population of fast ions. We clearly observe the dominant peak at $\omega \sim 2.5\omega_{d0}$ corresponding to the ion precession frequency for the toroidal number $n = 1$. Physical parameters of the simulation are beam density $n_b = 0.10n_0$, ion beam energy of $E_b = 10T_0$, ion temperature gradient of $\triangle\tau = 0.70$, and temperatures $T_e = T_i = T_0$.

been discussed in Ref. 1. In that work, a new approach was introduced based on the concept of phase-synchronization between several particles modes that represent different classes of particles distinguished by their level of "trapping" in tokamak's banana orbits. The strongly turbulent regime corresponds to a partial synchronization between different trapped particle modes (i.e., TIMs) excited by the initial ITG-instability and circulating ions (cf. Sec. IV). The second regime, dominated by auto-coherent phase-space structures, corresponds to a global synchronization among different modes involved, which phase-lock on an $n = 1$ mode that corresponds to a low-frequency zonal flow that, thus, provides a transport barrier. We have shown that the transition between the two regimes is induced by the presence of a small population of energetic particles (Sec. V). Although the analytical model that we have developed suggests that the transition depends on both the energetic particle density and energy, the numerical results that we have shown and discussed prove that the transition to a global synchronization can be induced by just increasing the energetic ion beam above a critical threshold value. A more systematic parameter study is required so to provide a determination of threshold values of experimental relevance. However, the analysis that we have developed and the preliminary results that we have shown indicate that for a given relative density of the energetic ion beam (n_b, in this article) with respect to that of the other circulating ions, the shift of the energy of the fast beam (E_b) with respect to energy of the bulk of circulating ions (E_+) exhibits a threshold, which plays a role equivalent to that of the coupling strength parameter $\tilde{\Gamma}_c$ of the Kuramoto-like model.

Albeit based on the simplifying assumption of a double gyroaverage over the fast time scales related to the cyclotron and the bounce or transit particle motion, the model introduced in Ref. 1 and here further discussed constitutes a complementary tool for first-principles simulations aimed at understanding the role played by ion-temperature-gradient instabilities over time scales comparable to those required for self-sustained, magnetically confined thermonuclear fusion experiments. Comparison with other paradigms of interaction between energetic particles and plasma modes also suggests that the synchronization model that we have discussed provides a

complementary way to look at other wave-particle interaction models. In particular, the transition from partial to global synchronization that we have shown for electrostatic ITG-driven modes seems analogous to the transition from a bump-on-tail to a fishbone scenario for electromagnetic instabilities (cf. Ref. 13). This invites to consider the possibility of interpreting also such scenarios in light of a synchronization model (Sec. VI).

Finally, beside of their general theoretical interest, we believe the results that we have discussed to be of relevance when investigating the suppression of tokamak turbulence by emergence of internal transport barriers induced by electron cyclotron resonance heating or by neutral beam injection (in the presence of TEM now).

ACKNOWLEDGMENTS

The authors are grateful to the IDRIS computational center, Orsay, France, for computer time allocation on their computers. This work was granted access to the HPC resources of IDRIS under Allocation Nos. A0110504028 and A0130504028 made by GENCI.

AUTHOR DECLARATIONS

Conflict of Interest

The authors have no conflicts to disclose.

DATA AVAILABILITY

The data that support the findings of this study are available from the corresponding author upon reasonable request.

APPENDIX: DERIVATION OF THE ENERGY CONSERVATION LAW FOR PARTICLE MODES

For the sake of completeness, the derivation of the energy conservation law for particle modes is here presented. The Hamiltonian associated with Vlasov equations (8) is $H_s = \omega_{ds}(E_s,\kappa)\psi + J_{0s}\phi$. It is then possible to decompose the total energy of particles, for a species s, into three distinct contributions: the kinetic energy $E_{kin,s}$, which depends on the type of particle modes (trapped or circulating); the energy of turbulence fluctuations driven by ITG-type instabilities, E_{turb}; and the zonal flow energy E_{ZF}. By writing the electric potential in the form $\phi = \langle\phi\rangle_\alpha + \delta\phi$, where $\langle.\rangle_\alpha = \int_0^{2\pi}\frac{d\alpha}{2\pi}$. expresses the average with respect to α, and after normalizing to $\omega_{d0}\triangle\psi$, the kinetic and turbulence energy components read as

$$E_{kin,s} = T_s\int_0^{2\pi}\frac{d\alpha}{2\pi}\int_0^1 d\psi\,\psi\langle\overline{\omega_{ds}}(E_s,\kappa)\rangle_{E_s,\kappa}, \tag{A1}$$

$$E_{turb} = \frac{1}{2}\int_0^{2\pi}\frac{d\alpha}{2\pi}\int_0^1 d\psi\left[C_e(1-f_p)\delta\phi^2 + f_pC_e|\bar{\nabla}\delta\phi|^2 + f_pC_i|\overline{\nabla}_i\delta\phi|^2 + \frac{1-f_p}{2}\sum_{\sigma_\parallel=\pm}C_i|\overline{\nabla}_{\sigma_\parallel}\delta\phi|^2\right], \tag{A2}$$

where $\bar{\mathbf{V}}_s = \rho^*\partial_\alpha\boldsymbol{e}_\alpha + \frac{\delta_s}{\triangle\psi}\partial_\psi\boldsymbol{e}_\psi$ is the normalized gradient in the $\psi-\alpha$ plane; $\delta_s = \{\delta_{be},\delta_{bi}\}$ for trapped particles and $\delta_s = \delta_{c\pm} \sim \sqrt{\varepsilon}\delta_{bi}$ for passing particles. Finally, the energy of the zonal flow reads

$$E_{ZF} = \frac{1}{2}\left[f_p\sum_{s=e,i}C_s\delta_{bs}^2 + \frac{1-f_p}{2}\sum_{\sigma_\parallel=\pm}C_i\delta_{c\pm}^2\right]\int_0^{2\pi}\frac{d\alpha}{2\pi}\int_0^1 d\psi\left(\frac{\partial\langle\phi\rangle_\alpha}{\partial\psi}\right)^2. \tag{A3}$$

In Eq. (A1), the quantity $\langle\overline{\omega_{ds}}(E_s,\kappa)\rangle_{E_s,\kappa}$ is determined by performing an integration over κ and E_s for trapped particles, so that

$$\langle\overline{\omega_{ds}}\rangle_{E_s,\kappa} = \frac{2}{\sqrt{\pi}}\int_0^1 d\kappa\,\kappa\,K(\kappa)\int_0^{+\infty}dE_i\sqrt{E_i}\,\overline{\omega_{ds}}(E_s,\kappa)\overline{f_s} \tag{A4}$$

while, for circulating ions, we have used

$$\langle\overline{\omega_{d,\pm}}\rangle_{E_s,\kappa} = \frac{2}{\sqrt{\pi}}\int_0^{+\infty}dE_i\sqrt{E_i}\int_1^{+\infty}d\kappa CK(\kappa^{-1})\overline{\omega_{d,\pm}}(E_i,\kappa)\overline{f_\pm}, \tag{A5}$$

with C being a constant that grants the distribution function to be normalized to one. Finally, a little algebra allows us to write the energy conservation law in the form

$$\frac{d}{dt}\left(\sum_{s\in\{e,i,\pm\}}E_{kin,s} + E_{turb} + E_{ZF}\right) = \Im(D), \tag{A6}$$

where the right-hand side of the equation $\Im$ contains the diffusion terms associated with the diffusion coefficient $D(\psi)$, introduced for numerical purposes so to increase the stability of the numerical scheme in the presence of strong turbulence. We have

$$\begin{aligned}\Im(D) = \Big\langle &\frac{3}{2}f_p\psi\frac{\partial}{\partial\psi}\left(D\frac{\partial}{\partial\psi}(P_i+P_e)\right) + \frac{3}{2}\frac{1-f_p}{2}\psi\frac{\partial}{\partial\psi}\left(D\frac{\partial}{\partial\psi}(P_+ + P_-)\right)\\ &+f_p\psi\frac{\partial}{\partial\psi}\left(D\frac{\partial}{\partial\psi}(n_i+n_e)\right) + \frac{1-f_p}{2}\psi\frac{\partial}{\partial\psi}\left(D\frac{\partial}{\partial\psi}(n_+ + n_-)\right)\Big\rangle_{\alpha,\psi},\end{aligned} \tag{A7}$$

where the symbols P_+ and P_-, respectively, refer to the pressure of the co-passing and counter-passing ion population, while P_i and P_e correspond to the pressure of trapped ions and electrons, respectively. A similar convention is used to represent the densities by n_s for a species $s = \{i,e,+,-\}$.

To conclude, the model of "particle modes" is a gyrokinetic model based on a double gyro-average on fast scales (both cyclotron plus bounce or transit fast scales), which introduces two classes of adiabatic invariants: energy E_s and pitch angle κ. The model consists of $N_{E_s}N_\kappa$ Vlasov equations, namely, Eq. (8) for N_{E_s} times N_κ values of adiabatic invariants (considered as parameters), coupled in a self-consistent way by the quasi-neutrality equation (11). The quasi-neutrality condition takes into account the standard corrections as polarization terms in (13). In Eq. (12), the trapped and circulating particle populations are defined, respectively, by

$$\overline{n_s}^{(t)} = \frac{2}{\sqrt{\pi}}\int_0^{+\infty}dE_s\sqrt{E_s}\int_0^1 d\kappa\kappa K(\kappa)\,J_{0s}^{(t)}\overline{f_{s,\kappa,E_s}}(\psi,\alpha,t) \tag{A8}$$

and

$$\sum_{\sigma_\parallel=\pm 1} \overline{n_{i,\sigma_\parallel}}^{(c)} = \frac{2}{\sqrt{\pi}} \int_0^{+\infty} dE_i \sqrt{E_i} \int_1^{+\infty} d\kappa C K(\kappa^{-1}) J_{0i}^{(c)} \left[\overline{f_i}^{+} + \overline{f_i}^{-} \right], \tag{A9}$$

where the normalization constant C grants the total circulating ion density to be equal to 1. In numerical simulations, the time is normalized to the inverse drift frequency $\omega_{d0}^{-1} = \frac{eB_0 r_0 R_0}{q_0 T_0}$ and the poloidal flux ψ is given in $\triangle\psi = \frac{r_0 R_0 B_0}{q_0}$ units, where B_0 is the minimal value of the magnetic field amplitude B_θ at $\theta = 0$; $R = R_0$ is the major radius and $r = r_0$ the minor radius of the tokamak; and $\varepsilon = \frac{r_0}{R_0}$ is the tokamak inverse aspect ratio. The electric potential ϕ, together with the constants C_e and C_i, is expressed in $\omega_{d0}\triangle\psi$ units.

REFERENCES

[1] A. Ghizzo and D. Del Sarto, "The model of particles modes I. A paradigm for phase synchronization in tokamak Turbulence," Phys. Plasmas (to be published).
[2] G. Depret, X. Garbet, P. Bertrand, and A. Ghizzo, Plasma Phys. Controlled Fusion **42**, 949 (2000).
[3] A. Ghizzo, D. Del Sarto, X. Garbet, and Y. Sarazin, Phys. Plasmas **17**, 092501 (2010).
[4] A. Pikovsky, M. Rosemblum, and J. Kurths, *Synchronization: A Universal Concept in Nonlinear Sciences* (Cambridge University Press, England, 2001).
[5] T. Stankovski, T. Pereira, P. V. E. McClintock, and A. Stefanovska, Rev. Mod. Phys. **89**, 045001 (2017).
[6] M. Leconte, Phys. Plasmas **26**, 072302 (2019).
[7] S. Xu, Z. B. Guo, and O. D. Gurcan, Phys. Rev. E **103**, 023208 (2021).
[8] F. Doveil, D. F. Escande, and A. Macor, Phys. Rev. Lett. **94**, 085003 (2005).
[9] Z. B. Guo, Y. H. Wang, and S. K. Xu, Phys. Rev. E **101**, 030201 (2020).
[10] Z. B. Guo, T. S. Hahm, and P. H. Diamond, Phys. Plasmas **22**, 122304 (2015).
[11] M. Sasaki, N. Kasuya, T. Kobayashi, H. Arakawa, K. Itoh, K. Fukunaga, T. Yamada, M. Yagi, and S.-I. Itoh, Phys. Plasmas **22**, 032315 (2015).
[12] K. J. Zhao, Y. Nagashima, P. H. Diamong, J. Q. Dong, K. Itoh, S. I. Itoh, L. W. Yang, J. Cheng, A. Fujisama, S. Inagaki, Y. Kosuga, M. Sasaki, Z. X. Wang, L. Wei, Z. H. Huang, D. L. Yu, W. Y. Hong, Q. Li, X. Q. Ji, X. M. Song, Y. Huang, Y. Liu, Q. W. Yang, X. T. Ding, and X. R. Duan, Phys. Rev. Lett. **117**, 145002 (2016).
[13] L. Chen and F. Zonca, Rev. Mod. Phys. **88**, 015008 (2016).
[14] M. Artun, W. M. Tang, and G. Rewoldt, Phys. Plasmas **2**, 3384 (1995).
[15] R. D. Sydora, V. K. Decyk, and J. M. Dawson, Plasma Phys. Controlled Fusion **38**, A281 (1996).
[16] R. Singh, P. Kaw, O. D. Gurcan, and P. H. Diamond, Phys. Plasmas **21**, 102306 (2014).
[17] T. Drouot, E. Gravier, T. Reveille, M. Sarrat, M. Collard, P. Bertrand, T. Cartier-Michaud, P. Ghendrih, Y. Sarazin, and X. Garbet, Phys. Plasmas **22**, 082302 (2015).
[18] E. Gravier, M. Lesur, T. Reveille, and T. Drouot, Phys. Plasmas **23**, 092507 (2016).
[19] A. Ghizzo, D. Del Sarto, F. Palermo, and A. Biancalani, Eur. Phys. Lett. **119**, 15003 (2017).
[20] A. Ghizzo and D. Del Sarto, Plasma **2**, 229 (2019).
[21] A. Strugarek, Y. Sarazin, D. Zarzoso, J. Abiteboul, A. S. Brun, T. Cartier-Michaud, G. Dif-Pradalier, X. Garbet, P. Ghendrih, V. Grandirard, G. Latu, C. Passeron, and O. Thomine, Plasma Phys. Controlled Fusion **55**, 074013 (2013).
[22] A. Strugarek, Y. Sarazin, D. Zarzoso, J. Abiteboul, A. S. Brun, T. Cartier-Michaud, G. Dif-Pradalier, X. Garbet, P. Ghendrih, V. Grandirard, G. Latu, C. Passeron, and O. Thomine, Phys. Rev. Lett. **111**, 145001 (2013).
[23] Y. Kuramoto and I. Nishikawa, J. Stat. Phys. **49**, 569 (1987).
[24] Y. Kuramoto, *Chemical Oscillations, Waves and Turbulence* (Springer-Verlag, Berlin, 1984).
[25] J. A. Acebron, L. L. Bonilla, C. J. Perez Vicente, F. Ritort, and R. Spigler, Rev. Mod. Phys. **77**, 137 (2005).
[26] S. T. Strogatz, Phys. D **143**, 1–20 (2000).
[27] L. F. Lafuerza, P. Colet, and R. Toral, Phys. Rev. Lett. **105**, 084101 (2010).
[28] O. E. Omel'Chenko and M. Wolfrum, Phys. Rev. Lett. **109**, 164101 (2012).
[29] G. Y. Fu, Phys. Rev. Lett. **101**, 185002 (2008).
[30] A. Si Siena, A. Banon Navarro, and F. Jenko, Phys. Rev. Lett. **125**, 105002 (2020).
[31] Y. Kolesnichenko, V. V. Lutsenko, V. S. Marchenko, and R. B. White, Phys. Plasmas **14**, 012504 (2007).
[32] A. Si Siena, R. Bilato, T. Gorler, A. Banon Navarro, E. Poli, V. Bobkov, D. Jarema, E. Fable, C. Angioni, Y. O. Kazakov, R. Ochoukov, P. Schneider, M. Weiland, F. Jenko, and ASDEX Upgrade Team, Phys. Rev. Lett. **127**, 025002 (2021).
[33] H. Cai, S. Wang, Y. Xu, J. Cao, and D. Li, Phys. Rev. Lett. **106**, 075002 (2011).
[34] E. Sonnendrucker, J. Roche, P. Bertrand, and A. Ghizzo, J. Comput. Phys. **149**, 201 (1999).
[35] A. Ghizzo, P. Bertrand, M. Shoucri, E. Fijalkow, and M. R. Feix, J. Comput. Phys. **108**, 105 (1993).
[36] P. H. Diamond, S. I. Itoh, and K. Itoh, *Modern Plasma Physics. Vol I. Physical Kinetics of Turbulent Plasmas* (Cambridge University Press, Cambridge, 2010).
[37] A. Ghizzo and D. Del Sarto, Plasma Phys. Controlled Fusion **63**, 055007 (2021).
[38] N. Winsor, J. L. Johnson, and J. M. Dawson, Phys. Fluids **11**, 2448 (1968).
[39] B. Scott, Phys. Lett. A **320**, 53 (2003).
[40] L. Chen, Phys. Plasmas **1**, 1519 (1994).
[41] K. Mc Guire, R. Goldston, M. Bell, M. Bitter, K. Bol, K. Brau, D. Buchenauer, T. Crowley, S. Davis, F. Dylla *et al.*, Phys. Rev. Lett. **50**, 891 (1983).
[42] R. B. White, R. J. Goldsteon, K. Mc Guire, A. H. Boozer, D. A. Monticello, and W. Park, Phys. Fluids **26**, 2958 (1983).
[43] H. L. Berk, C. W. Nielson, and K. W. Roberts, Phys. Fluids **13**, 980 (1970).
[44] T. M. O'Neil, J. H. Winfrey, and J. H. Malmberg, Phys. Fluids **14**, 1204 (1971).
[45] H. L. Berk, B. N. Breizmann, and H. Ye, Phys. Rev. Lett. **68**, 3563 (1992).
[46] T. M. Dupree, Phys. Fluids **15**, 334 (1972).
[47] R. H. Berman, D. J. Tetreault, and T. H. Dupree, Phys. Fluids **26**, 2437 (1983).
[48] I. B. Bernstein, J. M. Greene, and M. D. Kruskal, Phys. Rev. **108**, 546 (1957).
[49] A. Ghizzo, B. Izrar, P. Bertrand, E. Fijalkow, and M. R. Feix, Phys. Fluids **31**, 72 (1988).
[50] A. Ghizzo, B. Izrar, P. Bertrand, M. R. Feix, and E. Fijalkow, Phys. Lett. A **120**, 191 (1987).
[51] A. Ghizzo, M. Albrecht-Marc, T. Reveille, P. Bertrand, D. Del Sarto, and T. W. Johnston, Commun. Nonlinear Sci. Numer. Simul. **13**, 72 (2008).
[52] M. Albrecht-Marc, A. Ghizzo, T. Johnston, T. Reveille, D. Del Sarto, and P. Bertrand, Phys. Plasmas **14**, 072704 (2007).
[53] A. Ghizzo, M. M. Shoucri, P. Bertrand, M. R. Feix, and E. Fijalkow, Phys. Lett. A **129**, 453 (1988).